

Spectroscopic and Electronic Structure Studies of Copper(II) Binding to His111 in the Human Prion Protein Fragment 106–115: Evaluating the Role of Protons and Methionine Residues

Lina Rivillas-Acevedo, Rafael Grande-Aztatzi, Italia Lomelí, Javier E. García, Erika Barrios, Sarai Teloxa, Alberto Vela,* and Liliana Quintanar*

Departamento de Química, Centro de Investigación y de Estudios Avanzados (Cinvestav), 07360, D.F., Mexico

Received November 29, 2010

The prion protein (PrP^C) is implicated in the spongiform encephalopathies in mammals, and it is known to bind Cu(II) at the N-terminal region. The region around His111 has been proposed to be key for the conversion of normal PrP^C to its infectious isoform PrP^{Sc}. The principal aim of this study is to understand the role of protons and methionine residues 109 and 112 in the coordination of Cu(II) to the peptide fragment 106–115 of human PrP, using different spectroscopic techniques (UV–vis absorption, circular dichroism, and electron paramagnetic resonance) in combination with detailed electronic structure calculations. Our study has identified a proton equilibrium with a pK_a of 7.5 associated with the Cu(II)–PrP(106–115) complex, which is ascribed to the deprotonation of the Met109 amide group, and it converts the site from a 3NO to a 4N equatorial coordination mode. These findings have important implications as they imply that the coordination environment of this Cu binding site at physiological pH is a mixture of two species. This study also establishes that Met109 and Met112 do not participate as equatorial ligands for Cu, and that Met112 is not an essential ligand, while Met109 plays a more important role as a weak axial ligand, particularly for the 3NO coordination mode. A role for Met109 as a highly conserved residue that is important to regulate the protonation state and redox activity of this Cu binding site, which in turn would be important for the aggregation and amyloidogenic properties of the protein, is proposed.

Introduction

The prion protein (PrP^C) is a cell-surface monomeric glycoprotein that is responsible for a class of infectious neurodegenerative diseases known as transmissible spongiform encephalopathies (TSEs). These diseases include mad cow disease, scrapie in sheep, chronic wasting disease in elk and deer, and Creutzfeldt–Jakob disease in humans. TSEs are characterized by a structural modification of PrP^C to its infectious isoform named PrP^{Sc} or scrapie. Unlike the normal cellular form of the protein (PrP^C), PrP^{Sc} is rich in β -sheet structure, highly insoluble, protease-resistant and it readily forms aggregates and amyloid fibrils. These aggregates lead to the formation of neuronal plaques that have been associated with the induction of neuron apoptosis.^{1–3}

The biological function of PrP^C is not completely understood,^{4,5} however it has been demonstrated that PrP

displays high affinity toward Cu(II) in vivo,⁶ while there is growing evidence that PrP binds Zn(II) as well.^{7–9} Cellular studies show that Cu(II) and Zn(II) stimulate endocytosis of PrP,^{10,11} hence linking metal binding to a physiological response. Thus, it has been proposed that PrP may be involved in copper homeostasis or uptake into the cell,^{11,12} or it may possess a copper-dependent antioxidant function,^{13,14} possibly acting as a superoxide dismutase.¹⁵ It has also been proposed

(6) Brown, D. R.; Qin, K.; Herms, J. W.; Madlung, A.; Manson, J.; Strome, R.; Fraser, P. E.; Kruck, T.; von Bohlen, A.; Schulz-Schaeffer, W.; Giese, A.; Westway, D.; Kretschmar, H. A. *Nature* **1997**, *390*, 684–687.

(7) Brown, D. R.; Hafiz, F.; Glasssmith, L. L.; Wong, B.-S.; Jones, I. M.; Clive, C.; Haswell, S. J. *EMBO J.* **2000**, *19*, 1180–1186.

(8) Kenward, A. G.; Bartolotti, L. J.; Burns, C. S. *Biochemistry* **2007**, *46*, 4261–4271.

(9) Walter, E. D.; Stevens, D. J.; Visconte, M. P.; Millhauser, G. L. *J. Am. Chem. Soc.* **2007**, *129*, 15440–15441.

(10) Brown, L. R.; Harris, D. A. *J. Neurochem.* **2003**, *87*, 353–363.

(11) Pauly, P. C.; Harris, D. A. *J. Biol. Chem.* **1998**, *273*, 33107–33110.

(12) Sumudhu, W.; Perera, S.; Hooper, M. N. *Curr. Biol.* **2001**, *11*, 519–523.

(13) Klamt, F.; Dal-Pizzol, F.; Conte da Frota, M. L.; Walz, R.; Andrades, M. E.; Gomes da Silva, E.; Brentani, R. R.; Izquierdo, I.; Fonseca

Moreira, J. C. *Free Radical Biol. Med.* **2001**, *30*, 1137–1144.

(14) Nadal, R. C.; Abdelraheim, S. R.; Brazier, M. W.; Rigby, S. E. J.; Brown, D. R.; Viles, J. H. *Free Radical Biol. Med.* **2007**, *42*, 79–89.

(15) Brown, D. R.; Wong, B.-S.; Hafiz, F.; Clive, C.; Haswell, S. J.; Jones, I. M. *Biochem. J.* **1999**, *344*, 1–5.

*To whom correspondence should be addressed. Phone: +52-55-57473723. Fax: +52-55-57473389. E-mail: lilianaq@cinvestav.mx (L.Q.) or avela@cinvestav.mx (A.V.).

(1) Prusiner, S. B. *Science* **1982**, *216*, 136–144.

(2) Prusiner, S. B. *Science* **1991**, *252*, 1515–1522.

(3) Prusiner, S. B. *Science* **1997**, *278*, 245–251.

(4) Westergard, L.; Christensen, H. M.; Harris, D. A. *Biochim. Biophys. Acta* **2007**, *1772*, 629–644.

(5) Davis, P.; Brown, D. R. *Biochem. J.* **2008**, *410*, 237–244.

that PrP is involved in cell–cell adhesion¹⁶ and signal transduction¹⁷ and as an antiapoptosis agent.¹⁸

Nuclear magnetic resonance (NMR)^{19–21} and X-ray crystallography²² studies have indicated that PrP^C contains a predominantly α -helical structure at the C-terminal domain spanning residues 120–261, while the N-terminal domain is mostly unstructured.²³ It has been established that PrP^C can bind six Cu(II) ions in its flexible N-terminal region.^{24,25} Four Cu(II) ions bind to the region containing four repeats of the highly conserved octapeptide PHGGGWGQ sequence (residues 60–91 in the human sequence), while His96 and His111 have been identified as binding anchors in the region spanning residues 92–115.^{24–28} The octarepeat region binds copper in a series of different binding modes, depending on pH and the relative concentration of copper to protein.²⁹ X-ray crystallography, continuous wave and pulsed electron paramagnetic resonance (EPR) studies have shown that when there is enough Cu(II) each PHGGGWGQ fragment binds one Cu ion with a 3NO equatorial coordination mode at physiological pH. The binding site involves residues HGGGW, where the coordinating atoms are provided by the His imidazole ring, two deprotonated amide groups and a carbonyl moiety from the Gly residues that follow the His. A water molecule coordinates in the axial position to lead to a pentacoordinated Cu(II) complex that is stabilized by hydrogen bonding interactions with the Trp residue.^{24,30} Cu(II) binding to the octarepeat region has also been studied

extensively in the recent decade using electronic structure calculations and/or molecular dynamics.^{31–45}

While the coordination properties of Cu(II) bound to the octarepeat region have been revealed by very detailed spectroscopic and crystallographic studies, the nature of the Cu(II) coordination outside the octarepeat region has not been fully resolved. His96 and His111 have been recognized as the primary anchoring residues for Cu(II) binding^{28,46–48}, and the PrP(92–96) and PrP(106–113) fragments have been identified as the minimal sequences to reproduce Cu(II) binding to each of these His residues,^{25,27,49} however controversy still exists regarding the relevant Cu(II) coordination modes in the full protein. While some studies identify the His96 as the relevant Cu binding site²⁵ or the highest affinity site²⁷ in the 92–126 region, other studies have indicated a preference of Cu for binding at His111,^{47,50–53} while it has also been reported that Cu binds to each His site with equal affinity.⁴⁶ Finally, the formation of a Cu(II) complex involving coordination by both His residues cannot be ruled out, particularly at low pH.^{54–57}

Early EPR studies clearly demonstrated that Cu(II) binding to the PrP(92–96) fragment (with sequence GGGTH) involves the His96 imidazole and deprotonated amide groups from the preceding Thr and Gly residues.²⁵ Cu(II) binding at the His96 site is highly pH-dependent, and it can adopt a 3N1O or 4N equatorial coordination mode, depending on

(16) Mangé, A.; Milhavet, O.; Umlauf, D.; Harris, D.; Lehmann, S. *FEBS Lett.* **2002**, *514*, 159–162.

(17) Mouillet-Richard, S. M.; Ermonval, M.; Chebassier, C.; Laplanche, J. L.; Lehmann, S.; Launay, J. M.; Kellermann, O. *Science* **2000**, *289*, 1925–1928.

(18) Bounhar, Y.; Zhang, Y.; Goodyer, C. G.; LeBlanc, A. *J. Biol. Chem.* **2001**, *276*, 39145–39149.

(19) López García, F.; Zahn, R.; Riek, R.; Wüthrich, K. *Proc. Natl. Acad. Sci. U.S.A.* **2000**, *97*, 8334–8339.

(20) Zahn, R.; Liu, A.; Lührs, T.; Riek, R.; von Schroetter, C.; López García, F.; Billeter, M.; Calzolari, L.; Wider, G.; Wüthrich, K. *Proc. Natl. Acad. Sci. U.S.A.* **2000**, *97*, 145–150.

(21) Riek, R.; Hornemann, S.; Wider, G.; Billeter, M.; Glockshuber, R.; Wüthrich, K. *Nature* **1996**, *382*, 180–182.

(22) Haire, L. F.; Whyte, S. M.; Vasisth, N.; Gill, A. C.; Verma, C.; Dodson, E. J.; Dodson, G. G.; Bayley, P. M. *J. Mol. Biol.* **2004**, *336*, 1175–1183.

(23) Donne, D. G.; Viles, J. H.; Groth, D.; Mehlhorn, I.; James, T. L.; Cohen, F. E.; Prusiner, S. B.; Wright, P. E.; Dyson, J. H. *Proc. Natl. Acad. Sci. U.S.A.* **1997**, *94*, 13452–13457.

(24) Aronoff-Spencer, E.; Burns, C. S.; Avdievich, N. I.; Gerfen, G. J.; Peisach, J.; Antholine, W. E.; Ball, H. L.; Cohen, F. E.; Prusiner, S. B.; Millhauser, G. L. *Biochemistry* **2000**, *39*, 13760–13771.

(25) Burns, C. S.; Aronoff-Spencer, E.; Legname, G.; Prusiner, S. B.; Antholine, W. E.; Gerfen, G. J.; Peisach, J.; Millhauser, G. L. *Biochemistry* **2003**, *42*, 6794–6803.

(26) Qin, K.; Yang, Y.; Mastrangelo, P.; Westaway, D. *J. Biol. Chem.* **2002**, *277*, 1981–1990.

(27) Klewpatinond, M.; Davies, P.; Bowen, S.; Brown, D. R.; Viles, J. H. *J. Biol. Chem.* **2008**, *283*, 1870–1881.

(28) Jackson, G. S.; Murray, I.; Hosszu, L. L. P.; Gibbs, N.; Waltho, J. P.; Clarke, A. R.; Collinge, J. *Proc. Natl. Acad. Sci. U.S.A.* **2001**, *98*, 8531–8535.

(29) Chattopadhyay, M.; Walter, E. D.; Newell, D. J.; Jackson, P. J.; Aronoff-Spencer, E.; Peisach, J.; Gerfen, G. J.; Bennett, B.; Antholine, W. E.; Millhauser, G. L. *J. Am. Chem. Soc.* **2005**, *127*, 12647–12656.

(30) Burns, C. S.; Aronoff-Spencer, E.; Dunham, C. M.; Lario, P.; Avdievich, N. I.; Antholine, W. E.; Olmstead, M. M.; Vriehink, A.; Gerfen, G. J.; Peisach, J.; Scott, W. G.; Millhauser, G. L. *Biochemistry* **2002**, *41*, 3991–4001.

(31) Barry, S. D.; Rickard, G. A.; Pushie, M. J.; Rauk, A. *Can. J. Chem.* **2009**, *87*, 942–953.

(32) Bruschi, M.; De Gioia, L.; Mitric, R.; Bonacic-Koutecky, V.; Fantucci, P. *Phys. Chem. Chem. Phys.* **2008**, *10*, 4573–4583.

(33) Franzini, E.; DeGioia, L.; Fantucci, P.; Zampella, G.; Bonacic-Koutecky, V. *Inorg. Chem. Commun.* **2003**, *6*, 650–653.

(34) Ji, H.-F.; Zhang, H.-Y. *Chem. Res. Toxicol.* **2004**, *17*, 471–475.

(35) Pushie, J.; Rauk, A. *J. Biol. Inorg. Chem.* **2003**, *8*, 53–65.

(36) Riihimäki, E. S.; Kloo, L. *Inorg. Chem.* **2006**, *45*, 8509–8516.

(37) Riihimäki, E. S.; Martinez, J. M.; Kloo, L. *J. Mol. Struct. THEO-CHEM* **2006**, *760*, 91–98.

(38) Riihimäki, E. S.; Martinez, J. M.; Kloo, L. *J. Phys. Chem. B* **2007**, *111*, 10529–10537.

(39) Riihimäki, E. S.; Martinez, J. M.; Kloo, L. *Phys. Chem. Chem. Phys.* **2008**, *10*, 2488–2495.

(40) Guerrieri, F.; Minicozzi, V.; Morante, S.; Rossi, G.; Furlan, S.; La Penna, G. *J. Biol. Inorg. Chem.* **2009**, *14*, 361–374.

(41) Furlan, S.; La Penna, G.; Guerrieri, F.; Morante, S.; Rossi, G. C. *Eur. Biophys. J.* **2007**, *36*, 841–845.

(42) Furlan, S.; La Penna, G.; Guerrieri, F.; Morante, S.; Rossi, G. C. *J. Biol. Inorg. Chem.* **2007**, *12*, 571–583.

(43) Hodak, M.; Wenchang, L.; Bernholc, J. *J. Chem. Phys.* **2008**, *128*, 014101–9.

(44) Ames, W. M.; Larsen, S. C. *J. Biol. Inorg. Chem.* **2009**, *14*, 547–557.

(45) Pandey, K. K.; Snyder, J. P.; Liotta, D. C.; Musaev, D. G. *J. Phys. Chem. B* **2010**, *114*, 1127–1135.

(46) Walter, E. D.; Stevens, D. J.; Spevacek, A. R.; Visconte, M. P.; Dei Rossi, A.; Millhauser, G. L. *Curr. Protein Pept. Sci.* **2009**, *10*, 1–7.

(47) Osz, K.; Nagy, Z.; Pappalardo, G.; Di Natale, G.; Sanna, D.; Micera, G.; Rizzarelli, E.; Sövägö, I. *Chem.—Eur. J.* **2007**, *13*, 7129–7143.

(48) Kramer, M. L.; Kratzin, H. D.; Schmidt, B.; Römer, A.; Windl, O.; Liemann, S.; Hornemann, S.; Kretzschmar, H. *J. Biol. Chem.* **2001**, *276*, 16711–16719.

(49) Berti, F.; Gaggelli, E.; Guerrini, R.; Janicka, A.; Kozłowski, H.; Legowska, A.; Miecznikowska, H.; Migliorini, C.; Pogni, R.; Remelli, M.; Rolka, K.; Valensin, D.; Valensin, G. *Chem.—Eur. J.* **2007**, *13*, 1991–2001.

(50) Shearer, J.; Soh, P. *Inorg. Chem.* **2007**, *46*, 710–719.

(51) Thompsett, A. R.; Abdelrahim, S. R.; Daniels, M.; Brown, D. R. *J. Biol. Chem.* **2005**, *280*, 42750–42758.

(52) Remelli, M.; Valensin, D.; Bacco, D.; Gralka, E.; Guerrini, R.; Migliorini, C.; Kozłowski, H. *New J. Chem.* **2009**, *33*, 2300–2310.

(53) Di Natale, G.; Osz, K.; Nagy, Z.; Sanna, D.; Micera, G.; Pappalardo, G.; Sovago, I.; Rizzarelli, E. *Inorg. Chem.* **2009**, *48*, 4239–4250.

(54) Klewpatinond, M.; Viles, J. H. *Biochem. J.* **2007**, *404*, 393–402.

(55) Srikanth, R.; Wilson, J.; Burns, C. S.; Vachet, R. W. *Biochemistry* **2008**, *47*, 9258–9268.

(56) Wells, M. A.; Jackson, G. S.; Jones, S.; Hosszu, L. L. P.; Craven, J.; Clarke, A. R.; Collinge, J.; Waltho, J. P. *Biochem. J.* **2006**, *399*, 435–444.

(57) Jones, C. E.; Abdelrahim, S. R.; Brown, D. R.; Viles, J. H. *J. Biol. Chem.* **2004**, *279*, 32018–32027.

(58) Hureau, C.; Charlet, L.; Dorlet, P.; Gonnet, F.; Spadini, L.; Anxolabehere-Mallart, E.; Girerd, J.-J. *J. Biol. Inorg. Chem.* **2006**, *11*, 735–744.

pH.^{58,59} Regarding Cu(II) binding to His111, there is consensus that Lys residues are not involved in Cu binding,^{47,60–62} and that Cu(II) coordinates to the His imidazole ring and to a number of deprotonated amide groups from the backbone (one to three).^{25,47,50,54,57,60–64} However, there is controversy regarding the participation of the Met residues: based on circular dichroism (CD), EPR and NMR experiments it has been reported that no sulfur atoms participate in Cu(II) binding,^{60,62,63} while other groups propose Met coordination in the equatorial position, based on CD, EPR and X-ray absorption spectroscopy.^{50,61,64} Thus, the different proposals for equatorial coordination modes of Cu(II) bound to His111 at physiological pH include the following: 3NO with⁶² or without⁵⁴ two axial waters, 4N,^{25,54,61} 3NS,⁶¹ 2N2S and 2NSO with the participation of both Met109 and Met112 residues.^{50,64,65} Unfortunately the investigation of Cu(II) binding to His111 using electronic structure calculations has been scarce, and the only reports of electronic calculations for this site used overly simplified models for the amino acids that may participate in the coordination of the metal ion.^{64,66} Understanding Cu(II) binding to His111 is important, as this section of the protein is highly conserved in mammalian prion proteins,⁶⁷ and it has been identified as a key region in the structural modifications associated with the conversion of PrP^C to PrP^{Sc}, both experimentally⁶⁸ and by molecular dynamics.⁶⁹ Moreover, the PrP(106–126) fragment that contains His111 is highly fibrillogenic and neurotoxic in vitro,⁷⁰ it is protease resistant,⁷¹ it produces reactive oxygen species,⁷² and its Cu(II) complex has been shown to be redox active at physiological pH.⁵⁰

In this study we use different spectroscopic techniques (absorption, CD and EPR) in combination with electronic structure calculations to elucidate the coordination modes involved in Cu(II) binding to His111 in the PrP(106–115) fragment. A detailed pH study has allowed the identification

of two protonation states of the Cu(II)–peptide complex that coexist at physiological pH. The role of Met109 and Met112 in metal ion coordination has also been assessed by preparing peptide variants with Met to Ala substitutions and by evaluating different coordination modes using spin-unrestricted density functional theory (DFT) calculations. It is important to emphasize that all models used in the DFT calculations include all amino acid side chains for the PrP(106–113) fragment.

Experimental Section

N-Fluorenylmethoxycarbonyl (Fmoc) protected amino acids, Fmoc-Rink amide AM resin, and the hydroxybenzotriazole (HOBt) were obtained from Novabiochem (Switzerland); *N,N*-dimethylformamide (DMF) peptide synthesis grade was obtained from Fermont; *N,N*-diisopropylethylamine (DIEA), pyridine, *N,N*-diisopropylcarbodiimide (DIC), trifluoroacetic acid (TFA), tris(isopropyl)silane (TIS), ethanedithiol (EDT), acetonitrile (HPLC grade) and piperidine were obtained from Sigma (Saint Louis). All other chemicals were reagent grade and used without further purification. Water was purified to a resistivity of 18 MΩ/cm using a Millipore Gradient deionizing system.

Peptide Synthesis and Purification. The peptides KTNMKHMAGA (named PrP(106–115)), KTNMKH (PrP(106–111)), KTNMPHMAGA (PrP(106–115)K110P), KTNAKHMAGA (PrP(106–115)M109A), KTNMKHAAGA (PrP(106–115)M112A), and KTNAKHAAGA (PrP(106–115)M109A/M112A) were synthesized by solid-phase synthesis and Fmoc strategy, using Fmoc-Rink amide AM resin, as previously described.^{73,74} All peptides were acetylated at the amino terminus, and the carboxylic terminal was amidated. Crude peptides were purified by semipreparative reversed phase high performance liquid chromatography (HPLC). Peptide purity was determined by analytical HPLC and was found to be > 95%. The molecular weight of each peptide was determined by electrospray Ionization mass spectrometry (ESI-MS), and all purified products presented the expected molecular mass.

Preparation of Peptide Samples. Peptide solutions were prepared in 10 mM 2-(*N*-morpholino)ethanesulfonic acid (MES) buffer for pH 6.5, in 10 mM *N*-ethylmorpholine (NEM) for pH 7.5 and 8.5, or in a mixture of both buffers for pH dependence studies. For the pH titrations, the pH was varied every 0.25 unit by adding small volumes of NaOH or HCl solutions. Peptide samples for EPR spectroscopy were prepared in buffers with 50% glycerol to achieve adequate glassing. The addition of glycerol has no effect in the structure of the Cu(II)–peptide complexes, as evaluated by absorption and circular dichroism spectroscopy for all buffer solutions and pH values used in this study. The absorption coefficient for each peptide at 214 nm was determined in each buffer solution at pH 6.5, 7.5 and 8.5, and it was found to be buffer- and pH- independent. These absorption coefficients were used to determine the concentration of peptide in each sample that was analyzed. Final peptide concentrations were in the order of 0.5 mM.

UV–Visible Absorption and Circular Dichroism (CD) Spectroscopy. Room temperature absorption and CD spectra were recorded using an Agilent 8453 diode array spectrometer and a Jasco J-815 CD spectropolarimeter, respectively. Spectra were recorded in quartz cells with either 1 or 0.1 cm path lengths. Gaussian fitting of the absorption and CD spectra were performed using PeakFit 4.0 (Jandel). Gaussian analyses of the absorption and CD spectra were performed as followed: the same parameters (energy and bandwidth) were used to fit both

(59) Hureau, C.; Mathe, C.; Faller, P.; Mattioli, T. A.; Dorlet, P. *J. Biol. Inorg. Chem.* **2008**, *13*, 1055–1064.

(60) Belosi, B.; Gaggelli, E.; Guerrini, R.; Kozłowski, H.; Luczkowski, M.; Mancini, F. M.; Remelli, M.; Valensin, D.; Valensin, G. *ChemBioChem* **2004**, *5*, 349–359.

(61) DiNatale, G.; Grasso, G.; Impellizzeri, G.; LaMendola, D.; Micera, G.; Mihala, N.; Nagy, Z.; Osz, K.; Pappalardo, G.; Rigo, V.; Rizzarelli, E.; Sanna, D.; Sovago, I. *Inorg. Chem.* **2005**, *44*, 7214–7225.

(62) Remelli, M.; Donatoni, M.; Guerrini, R.; Janicka, A.; Pretegianni, P.; Kozłowski, H. *Dalton Trans.* **2005**, *17*, 2876–2885.

(63) Gaggelli, E.; Bernardi, F.; Molteni, E.; Pogni, R.; Valensin, D.; Valensin, G.; Remelli, M.; Luczkowski, M.; Kozłowski, H. *J. Am. Chem. Soc.* **2005**, *127*, 996–1006.

(64) Shearer, J.; Soh, P.; Lentz, S. *J. Inorg. Biochem.* **2008**, *102*, 2103–2113.

(65) Jobling, M. F.; Huang, X.; Stewart, L. R.; Barnham, K. J.; Curtain, C.; Volitakis, I.; Perugini, M.; White, A. R.; Cherny, R. A.; Masters, C. L.; Barrow, C. J.; Collins, S. J.; Bush, A. I.; Cappai, R. *Biochemistry* **2001**, *40*, 8073–8084.

(66) Yamamoto, N.; Kuwata, K. *Chem. Phys. Lett.* **2010**, *498*, 184–187.

(67) Wopfner, F.; Weidenhöfer, G.; Schneider, R.; von Brunn, A.; Gilch, S.; Schwarz, T. F.; Werner, T.; Schätzl, H. M. *J. Mol. Biol.* **1999**, *289*, 1163–1178.

(68) Prusiner, S. B. *Proc. Natl. Acad. Sci. U.S.A.* **1998**, *95*, 13363–13383.

(69) Moro, G.; Bonati, L.; Bruschi, M.; Cosentino, U.; De Gioia, L.; Fantucci, P. C.; Pandini, A.; Papaleo, E.; Pitea, D.; Saracino, G. A. A.; Zampella, G. *Theor. Chem. Acc.* **2007**, *117*, 723–741.

(70) Forloni, G.; Angeretti, N.; Chiesa, R.; Monzani, E.; Salmons, M.; Bugiani, O.; Tagliavini, F. *Nature* **1993**, *362*, 543–546.

(71) Selvaggini, C.; De Gioia, L.; Cantù, L.; Ghibaudi, E.; Diomedea, L.; Passerini, F.; Forloni, G.; Bugiani, O.; Tagliavini, F.; Salmons, M. *Biochem. Biophys. Res. Commun.* **1993**, *194*, 1380–1386.

(72) Turnbull, S.; Tabner, B. J.; Brown, D. R.; Allsop, D. *Neurosci. Lett.* **2003**, *336*, 159–162.

(73) Kates, E.; Albericio, F. *Solid-Phase Synthesis*; Marcel Dekker Inc.: New York, 2000.

(74) Hood, C. A.; Fuentes, G.; Patel, H.; Page, K.; Menakuru, M.; Park, J. *J. Pept. Sci.* **2008**, *14*, 97–101.

the absorption and CD in order to help constrain the fit. The minimum number of bands was used to adequately fit key features in both spectra.

Electron Paramagnetic Resonance (EPR) Spectroscopy. X-band EPR spectra were collected using an EMX Plus Bruker System, with an ER 041 XG microwave bridge and an ER 4102ST cavity. The following conditions were used: microwave power, 10 mW; modulation amplitude, 5 G; modulation frequency, 100 kHz; time constant, 327 ms; conversion time, 82 ms; and averaging over 18 scans. EPR spectra were recorded either at 77 K using a finger quartz dewar with liquid nitrogen, or at 150 K using a ER4131VT variable temperature nitrogen system. For experiments performed in ^{17}O water, the buffer solution (10 mM MES) was prepared with 60–70% enriched H_2^{17}O (Cambridge Isotopes) and 30% glycerol to achieve adequate glassing. The peptide was dissolved in this solution at a final concentration of 1 mM, 0.5 equiv of Cu(II) were added and the pH of the final solution was adjusted using a microelectrode and a solution of NaOH in 60–70% enriched H_2^{17}O . A peptide sample in ^{16}O water was prepared in parallel using the same protocol for each experiment. X-band EPR spectra of these samples were collected at 20 K using an ER4112HV continuous flow liquid helium cryostat, and the following conditions: microwave frequency, 9.4 GHz; microwave power, 1 mW; modulation amplitude, 5 G; modulation frequency, 100 kHz; time constant, 327 ms; conversion time, 82 ms; and averaging over 6 scans. EPR spectra were baseline-corrected and simulated using WinEPR SimFonia and XSophe programs (Bruker).

Electronic Structure Calculations. For all calculations, the PrP(106–113) peptide with sequence KTNMKHMA was used, with an acetylated N-terminus and the C-terminal amidated, in order to best resemble the peptide used to collect the experimental data. Each model for the Cu(II)–peptide complex was constructed in Molden,⁷⁵ starting with the optimized structure of the free peptide. The structures had a total of 140 to 148 atoms, depending on the protonation state of the backbone amides and the number of explicit water molecules included in each model. Using an unrestricted Kohn–Sham (UKS) approach, all Cu(II)–peptide complex structures with a spin multiplicity of two (doublet) were fully optimized without any geometry constraints and the stationary points were characterized by a harmonic analysis. All geometry optimizations were performed using the deMon2k code⁷⁶ at the local level with the Dirac⁷⁷–VWN⁷⁸ exchange–correlation functional, and also with the functional PBE⁷⁹ of the family of generalized gradient approximation. These functionals were selected because they are nonempirical and belong to the first two rungs of Jacob’s ladder;⁸⁰ thus, a comparison of their results sheds light on the role of the functional in the description of these complex molecular systems. DZVP⁸¹ and GEN-A2 were used as orbital and auxiliary basis sets, respectively, avoiding the evaluation of

four center integrals by invoking the variational fitting of the Coulomb energy.^{82,83} Solvent effects on the optimized structures were calculated using the implicit solvation model COSMO,^{84,85} as implemented in the ORCA program.⁸⁶ EPR parameters, \mathbf{g} and \mathbf{A} tensors, of the optimized structures were calculated with ORCA using the nonempirical hybrid functional PBE0,⁸⁷ the CP basis⁸⁸ for the copper atom, and in all other atoms DGAUSS was used. IGLO⁸⁹ was used as the gauge origin and COSMO was also employed. Some EPR parameter calculations were also performed using the EPRIII basis⁹⁰ on nitrogen and oxygen atoms, but no significant changes in the \mathbf{g} and \mathbf{A} tensor values were observed.

Results and Analysis

1. Cu(II) Binding to the PrP(106–115) Fragment: Evaluating the Role of Protons. **1.1. Cu(II) Binding to PrP(106–115) Followed by UV–Vis Absorption and Circular Dichroism (CD).** A 0.5 mM solution of PrP(106–115) was titrated with Cu(II) at different pH values, and the titrations were followed simultaneously by UV–vis absorption and CD. The absorption data at pH 8.5 (Figure 1A) show the growth of a signal at $\approx 39000\text{ cm}^{-1}$ ($\epsilon \approx 4000\text{ M}^{-1}\text{ cm}^{-1}$) with a shoulder at $\approx 31000\text{ cm}^{-1}$, and a smaller band centered around 17500 cm^{-1} ($\epsilon \approx 80\text{ M}^{-1}\text{ cm}^{-1}$) upon addition of Cu(II). The CD spectra (Figure 1B) show the growth of signals at $\approx 38500\text{ cm}^{-1}$ ($\Delta\epsilon \approx 5\text{ M}^{-1}\text{ cm}^{-1}$) and at 31600 cm^{-1} ($\Delta\epsilon \approx 0.7\text{ M}^{-1}\text{ cm}^{-1}$); while the band observed by absorption at 17500 cm^{-1} (Figure 1A, inset) gets resolved by CD into a positive signal at 15800 cm^{-1} and a negative signal at 20200 cm^{-1} (Figure 1B, inset). All signals saturate after 1 equiv of Cu(II) has been added (data not shown). The titration of the PrP(106–115) fragment at pH 7.5 followed by UV–vis absorption (Figure 1C) and CD (Figure 1D) displays very similar signals to those observed at pH 8.5. However, the lower energy region of the CD spectra (Figure 1D, inset) shows four bands: a negative signal at $\approx 12900\text{ cm}^{-1}$, a positive signal at $\approx 15800\text{ cm}^{-1}$, a small positive shoulder at $\approx 18000\text{ cm}^{-1}$, and a negative signal at $\approx 20500\text{ cm}^{-1}$. The titration performed at pH 6.5 followed by UV–vis absorption (Figure 1E) and CD (Figure 1F) displays similar signals to those observed at higher pH values. The main differences are evident in the CD spectra: a negative band is present at 30400 cm^{-1} , and the lower energy region (Figure 1F, inset) displays two bands: a negative signal at $\approx 13000\text{ cm}^{-1}$ and a positive signal at $\approx 18500\text{ cm}^{-1}$. Finally, the CD data collected at pH 5.5 displays signals that are very similar to those observed at pH 6.5, but they display much lower intensity, while the UV absorption data show signals that correspond to free Cu(II) in solution (data not shown). These results indicate that the affinity of Cu(II) for the PrP(106–115) fragment is

(75) Schaftenaar, G.; Noordik, J. H. *J. Comput.-Aided Mol. Des.* **2000**, *14*, 123–134.

(76) Köster, A. M.; Calaminici, P.; Casida, M. E.; Dominguez, V. D.; Flores-Moreno, R.; Geudtner, G.; Goursot, A.; Heine, T.; Ipatov, A.; Janetzko, F.; Campo, J. M. d.; Patchkovskii, S.; Reveles, J. U.; Zuñiga, B.; Vela, A.; Salahub, D. R. *deMon2k*, 2.5.1; The International deMon Developers: Mexico D.F., Mexico, 2009.

(77) Dirac, P. A. M. *Proc. Cambridge Philos. Soc.* **1930**, *26*, 376–385.

(78) Vosko, S. H.; Wilk, L.; Nusair, M. *Can. J. Phys.* **1980**, *58*, 1200–1211.

(79) Perdew, J. P.; Burke, K.; Ernzerhof, M. *Phys. Rev. Lett.* **1996**, *77*, 3865–3868.

(80) Perdew, J. P.; Schmidt, K. Citation to Jacobs Ladder (Taken from JPP papers). In *Density Functional Theory and Its Applications to Materials*; Doren, V. V.; Alsenoy, C. V., Eds.; AIP: Melville, NY, 2001.

(81) Godbout, N.; Salahub, D. R.; Andzelm, J.; Wimmer, E. *Can. J. Chem.* **1992**, *70*, 560–571.

(82) Dunlap, B. I.; Connolly, J. W. D.; Sabin, J. R. *J. Chem. Phys.* **1979**, *71*, 3396–3402.

(83) Koster, A. M.; del Campo, J. M.; Janetzko, F.; Zuniga-Gutierrez, B. *J. Chem. Phys.* **2009**, *130*.

(84) Klamt, A.; Schuurmann, G. *J. Chem. Soc., Perkin Trans. 2* **1993**, 799–805.

(85) Sinnecker, S.; Rajendran, A.; Klamt, A.; Diedenhofen, M.; Neese, F. *J. Phys. Chem. A* **2006**, *110*, 2235–2245.

(86) Neese, F. *ORCA—an ab initio density functional and semiempirical program package*, Version 2.6, rev. 35; University of Bonn: 2008.

(87) Adamo, C.; Barone, V. *J. Chem. Phys.* **1999**, *110*, 6158–6170.

(88) The ORCA basis set “CoreProp” was used. This basis is based on the TurboMole DZ basis developed by Ahlrichs and co-workers and obtained from the basis set library under ftp.chemie.unikarlsruhe.de/pub/basen.

(89) Kutzelnigg, W.; Fleischer, U.; Schindler, M. *The IGLO-Method: Ab Initio Calculation and Interpretation of NMR Chemical Shifts and Magnetic Susceptibilities*; Springer-Verlag: Heidelberg, 1990; Vol. 23.

(90) Barone, V. In *Recent Advances in Density Functional Methods, Part I*; Chong, D. P., Ed.; World Scientific Pub. Co.: Singapore, 1996.

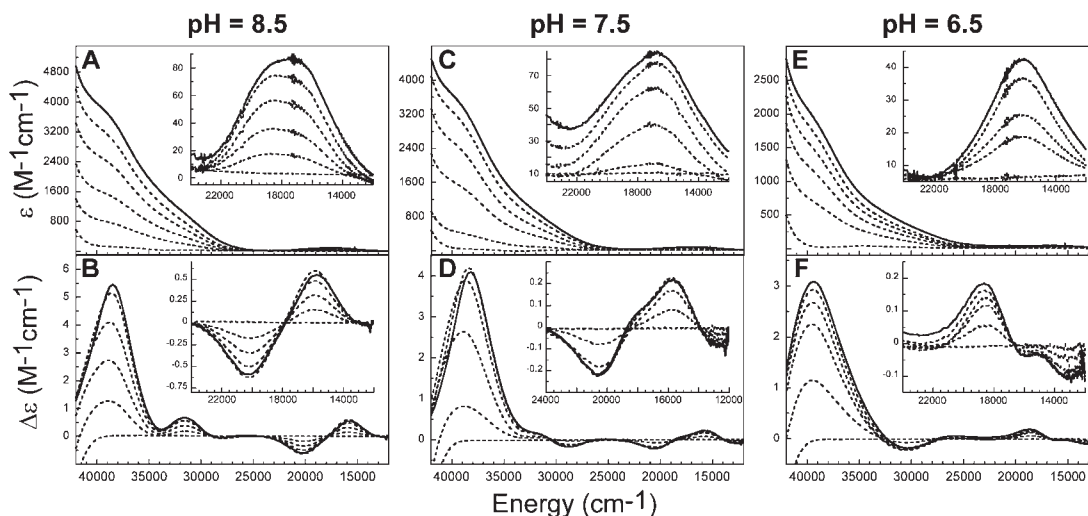


Figure 1. Titration of the PrP(106–115) fragment with Cu(II) as followed by UV–vis absorption at pH 8.5 (A), 7.5 (C) and 6.5 (E); and by circular dichroism at pH 8.5 (B), 7.5 (D) and 6.5 (F). Only the spectra recorded after the addition of 0, 0.2, 0.4, 0.6, 0.8 equiv (all in dotted lines), and 1.0 equiv (solid lines) of Cu(II) are displayed. A close-up of the lower energy region is shown in the inset for each figure.

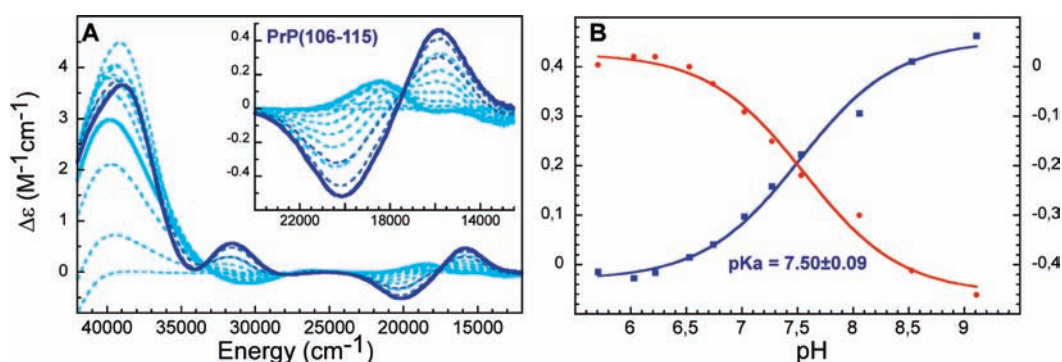


Figure 2. pH titration of the Cu(II) complex with PrP(106–115) (A) as followed by circular dichroism. The Cu(II) complex solutions were titrated from pH \sim 5.5 (thick light color line) to pH \sim 9.5–10 (thick dark line); spectra for intermediate pH values are shown in dashed lines. The traces for the CD signal intensity changes at 15800 cm^{-1} (blue) and 20800 cm^{-1} (red) (B) for the Cu(II) complex with PrP(106–115) were fit to the model described in the text (solid lines) to determine the associated $\text{p}K_a$.

significantly decreased at pH 5.5, probably due to protonation of His111.

From a close inspection and comparison of the CD spectra of the Cu(II) complexes at pH 8.5, 7.5, and 6.5 (insets of Figures 1B, 1D and 1F, respectively), it becomes clear that the d–d region of the spectrum changes dramatically: from a negative signal at \approx 13000 cm^{-1} and a positive signal at \approx 18500 cm^{-1} at pH 6.5, to a positive signal at 15800 cm^{-1} and a negative signal at 20200 cm^{-1} at pH 8.5. Moreover, the CD spectrum of the Cu(II) complex at pH 7.5 can be deconvoluted as a mixture of the spectra at pH 6.5 and 8.5 (Figure S1 in the Supporting Information). This observation suggests that there may be a proton equilibrium associated with the observed signal changes, and that at pH 7.5 the CD spectrum is allowing the detection of at least two species with different protonation states.

1.2. The Effect of pH on the Cu(II) Coordination to the PrP(106–115) Peptide, as Followed by CD. In order to further evaluate the changes observed in the CD spectrum of the Cu(II)–PrP(106–115) complex upon pH, 1 equiv of Cu(II) was added to a 0.5 mM solution of peptide, and a pH titration was followed by CD (Figure 2A). The most dramatic changes occur in the lower energy region of the

CD spectra (Figure 2A, inset). Following the CD spectral changes at 15800 cm^{-1} and at 20833 cm^{-1} (Figure 2B), it becomes evident that the signal intensity is dependent on pH and it displays a sigmoidal behavior, which is indicative of a single protonation equilibrium. The experimental data could be best fit with the following model:

$$\Delta\epsilon_{\text{obs}} = (\Delta\epsilon_{\text{lowpH}}[\text{H}^+] + \Delta\epsilon_{\text{highpH}}K_a) / (K_a + [\text{H}^+])$$

where $\Delta\epsilon_{\text{obs}}$ is the observed CD signal intensity at any given pH, K_a is the equilibrium constant associated with the protonation equilibrium of the Cu(II)–peptide complex, $\Delta\epsilon_{\text{lowpH}}$ is the CD signal intensity associated with the protonated form of the complex, and $\Delta\epsilon_{\text{highpH}}$ is the CD signal intensity associated with its deprotonated form. The $\text{p}K_a$ associated with the protonation of the Cu(II)–PrP(106–115) complex is 7.50 ± 0.09 , as determined by the best fit of experimental data derived from at least triplicate experiments.

In order to further characterize the protonated and deprotonated forms of the Cu(II)–PrP(106–115) complex, simultaneous Gaussian analysis of their absorption and CD spectra was performed. The absorption and CD spectra of both forms can be resolved into seven

Table 1. Parameters of the Gaussian Fits of Absorption and CD Spectra of the Cu(II)–PrP(106–115) Complex at pH 8.5 and 6.5

band no.	pH 8.5		pH 6.5	
	energy ^a	$\Delta\epsilon/\epsilon^b$	energy ^a	$\Delta\epsilon/\epsilon^b$
1 d → d	15858	9.90	12935	–11.3
2 d → d	18474	–2.36	16155	–1.03
3 d → d	20534	–24.3	18692	31.2
4 S _{Met} σ → Cu CT	28580	–1.29	26594	4.89
5 N [–] _{amide} → Cu CT	31567	1.10	30270	–1.06
6 N _{im} π ₁ → Cu CT	35891	0.493	35390	0.93
7 N _{im} π ₂ → Cu CT	38535	2.27	39600	2.15

^aThe energy of the transitions is reported in cm^{–1}. The energy was obtained from simultaneously fitting of CD and absorption spectra. ^bKuhn anisotropy factor calculated from the CD intensity ($\Delta\epsilon$) in M^{–1} cm^{–1} and the absorption intensity (ϵ) in M^{–1} cm^{–1}, and expressed as $X \times 10^{-3}$.

transitions with the energies listed in Table 1, as shown in Figure 3. On the basis of their high Kuhn anisotropy factors (ratio of CD to absorption intensity, $\Delta\epsilon/\epsilon$, Table 1), bands 1–3 can be assigned as ligand field (d–d) transitions, while bands 4–7 can be assigned as ligand-to-metal charge transfer (LMCT) transitions. The resolution of three d–d transitions is consistent with having a Cu(II) complex with a distorted square planar geometry. The maximum λ for the ligand field envelope in the absorption spectrum at pH 8.5 is ~18000 cm^{–1} (with $\epsilon \sim 80$ cm^{–1} M^{–1}), as found for Cu(II)–peptide complexes that involve the coordination of His and three deprotonated amide groups.^{91,92} At pH 6.5, the ligand field envelope is centered around ~16000 cm^{–1} (with $\epsilon \sim 40$ cm^{–1} M^{–1}), consistent with a Cu(II)–peptide complex that involves the coordination of His and one or two deprotonated amide groups.^{91,92} The interaction of Cu(II) with the imidazole nitrogen of His111 is expected to generate two π (π_1 and π_2) → Cu(II) charge transfer (CT) transitions and one σ → Cu(II) CT transition. Studies of tetra-coordinated Cu(II)–imidazole and Cu(II)–peptide complexes have shown that the π_1 → Cu(II) CT transitions originate from a mostly carbon-based orbital and appear at lower energy (27000 to 35700 cm^{–1}) than the π_2 → Cu(II) transitions (32500 to 40800 cm^{–1}), which originate from a mostly nitrogen-based orbital.^{93–95} Moreover, studies of Cu(II)–peptide complexes have shown that the participation of deprotonated backbone amide groups in the metal ion coordination generates a N[–] → Cu(II) CT transition at 31000 to 34000 cm^{–1} with relatively low intensity ($\Delta\epsilon \sim 0.2$ cm^{–1} M^{–1} per deprotonated amide).^{94,96,97} Thus, LMCT bands number 6 and 7 in Figure 3 and Table 1 can be assigned to the π_1 → Cu(II) and π_2 → Cu(II) CT transitions, respectively; while LMCT transition number 5 can be assigned to a N[–] → Cu(II) CT transition. Finally, LMCT band number 4

appears in the energy range where S → Cu(II) CT transitions have been identified in Cu(II) complexes with Met-containing peptides (27700 to 30300 cm^{–1}).⁹⁶ However, given the low intensity of band 4, equatorial Cu(II)–thioether bonding can be discarded,^{98–102} and band 4 may be indicative of weak Met sulfur coordination in an axial position.^{102,103}

1.3. The Effect of pH on the Cu(II) Coordination to the PrP(106–115) Peptide, as Followed by X-Band Electron Paramagnetic Resonance (EPR). PrP(106–115) was titrated by Cu(II) at pH 8.5 and 6.5, as followed by X-band EPR (data not shown). In all cases, the EPR spectra display $g_{\perp} > g_{\parallel} > 2.00$ and a large parallel hyperfine splitting, which is indicative of a d_{x²–y²} ground state. The X-band EPR spectrum of the Cu(II) complex with PrP(106–115) at pH 8.5 is shown in Figure 4A. The g_{\parallel} value = 2.199 and hyperfine splitting $A_{\parallel} = 191 \times 10^{-4}$ cm^{–1} associated with this complex fall close to the range of values associated with a 4N equatorial coordination mode,^{104,105} and they are similar for other reported Cu(II) complexes with 4N coordination modes.⁵⁸ Thus, it is likely that the Cu(II)–PrP(106–115) complex at pH 8.5 holds a 4N equatorial coordination mode, although a 3N1O coordination mode cannot be excluded from these EPR data only. Evaluation of plausible models for the deprotonated form of the Cu(II)–PrP(106–115) complex by DFT calculations (section 4) supports the assignment as a 4N mode. The EPR spectrum of the complex at pH 8.5 was simulated (Figure 4A) using the parameters listed in Table S1 in the Supporting Information. In order to accurately simulate the fine structure in the perpendicular region of the spectrum, the use of a set of four nonequivalent nitrogens was needed. The rhombicity of the site (i.e., $g_x \neq g_y$) suggests that the four equatorial nitrogen ligands involved in the metal ion coordination are not equivalent, as it is evidenced by DFT calculations (section 4.5).

The EPR titration performed at pH 6.5 shows the growth of a set of EPR signals assigned to peptide-bound Cu(II), while, after the addition of 0.75 equiv of Cu(II), a second set of EPR signals becomes evident, and they correspond to Cu(II) in solution (data not shown). This observation is indicative of a lower affinity of Cu(II) for the peptide at this pH. Figure 4B displays the X-band EPR spectrum of the PrP(106–115) peptide after the addition of 0.5 equiv of Cu(II) at pH 6.5. The EPR signal assigned to the Cu(II)–peptide complex has a g_{\parallel} value of 2.226 and a hyperfine splitting of $A_{\parallel} = 167 \times 10^{-4}$ cm^{–1};

(98) Gilbert, J. G.; Addison, A. W.; Nazarenko, A. Y.; Butcher, R. J. *Inorg. Chim. Acta* **2001**, *324*, 123–130.

(99) Miskowski, V. M.; Thich, J. A.; Solomon, R.; Schugar, H. J. *J. Am. Chem. Soc.* **1976**, *98*, 8344–8350.

(100) Lee, Y.; Lee, D.-H.; Narducci Sarjeant, A. A.; Zakharov, L. N.; Rheingold, A. L.; Karlin, K. D. *Inorg. Chem.* **2006**, *45*, 10098–10107.

(101) Nikles, D. E.; Powers, M. J.; Urbach, F. L. *Inorg. Chem.* **1983**, *22*, 3210–3217.

(102) Amundsen, A. R.; Whelan, J.; Bosnich, B. *J. Am. Chem. Soc.* **1977**, *99*, 6730–6739.

(103) Prochaska, H. J.; Schwindinger, W. F.; Schwartz, M.; Burk, M. J.; Bernarducci, E.; Lalancette, R. A.; Potenza, J. A.; Schugar, H. J. *J. Am. Chem. Soc.* **1981**, *103*, 3446–3455.

(104) Peisach, J.; Blumberg, W. E. *Arch. Biochem. Biophys.* **1974**, *165*, 691–708.

(105) Sakaguchi, U.; Addison, A. W. *J. Chem. Soc., Dalton Trans.* **1979**, 600–608.

(91) Bryce, G. F.; Gurd, F. R. N. *J. Biol. Chem.* **1966**, *241*, 122–129.

(92) Bryce, G. F.; Roeske, R. W.; Gurd, F. R. N. *J. Biol. Chem.* **1966**, *241*, 1072–1080.

(93) Bernarducci, E. E.; Schwindinger, W. F.; Hughey, J. L.; Krogh-Jespersen, K.; Schugar, H. J. *J. Am. Chem. Soc.* **1981**, *103*, 1686–1691.

(94) Daniele, P. G.; Prenesti, E.; Ostacoli, G. *J. Chem. Soc., Dalton Trans.* **1996**, 3269–3275.

(95) Fawcett, T. G.; Bernarducci, E. E.; Krogh-Jespersen, K.; Schugar, H. J. *J. Am. Chem. Soc.* **1980**, *102*, 2598–2604.

(96) Osz, K.; Boka, B.; Varnagy, K.; Sovago, I.; Kurtan, T.; Antus, S. *Polyhedron* **2002**, *21*, 2149–2159.

(97) Varnagy, K.; Boka, B.; Sovago, I.; Sanna, D.; Marras, P.; Micera, G. *Inorg. Chim. Acta* **1998**, *275–276*, 440–446.

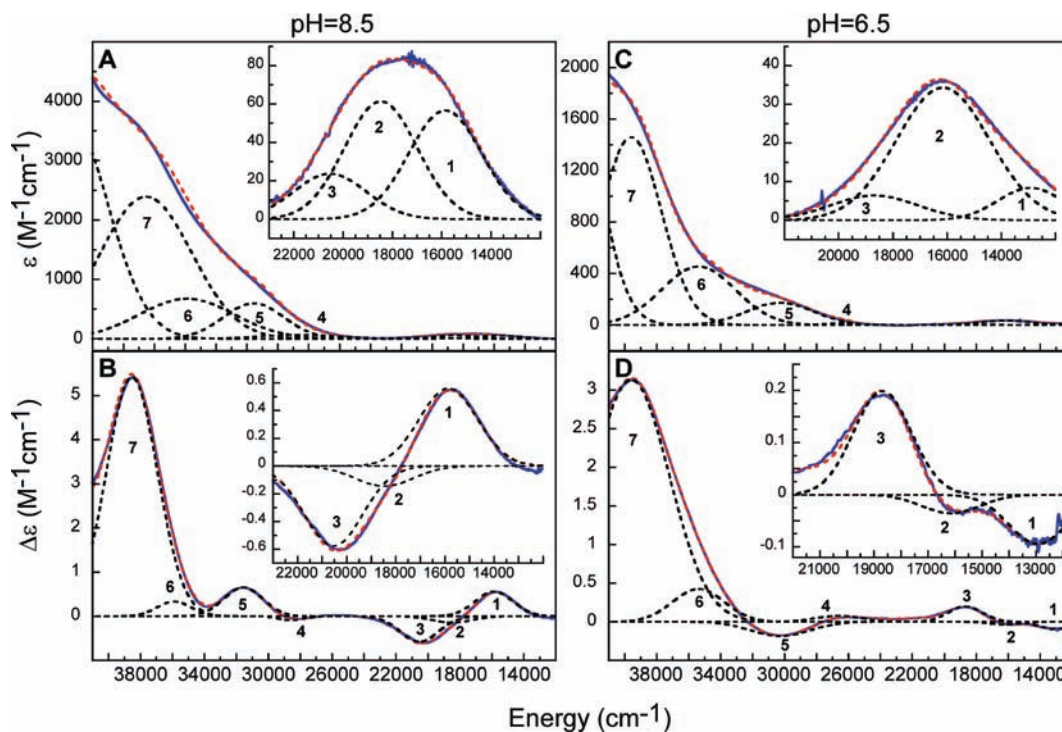


Figure 3. Gaussian fits of the UV-vis absorption (A and C) and circular dichroism (B and D) spectra of the Cu(II)-PrP(106-115) complex at pH 8.5 and at pH 6.5, respectively. Experimental spectra (blue), Gaussian fits (red), and individual Gaussian bands (dotted lines) with the parameters listed in Table 1 are shown.

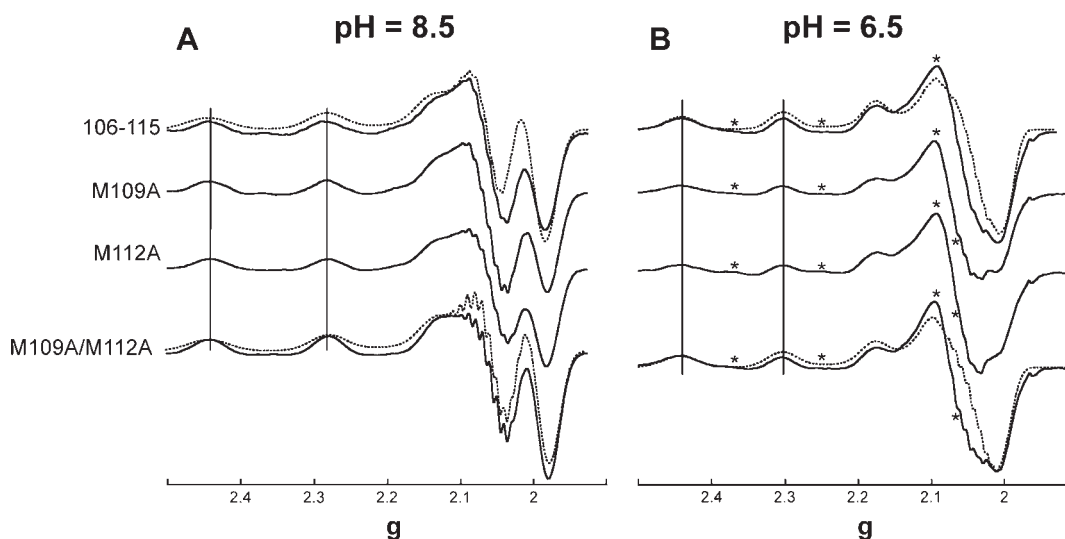


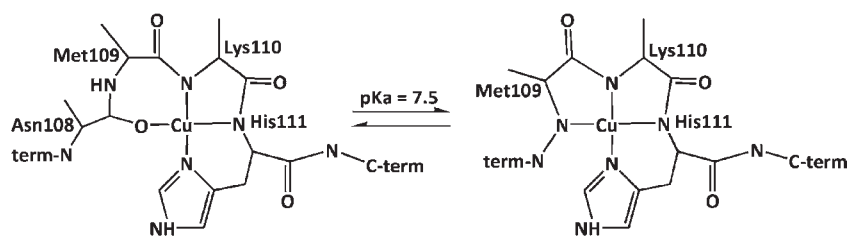
Figure 4. EPR spectra of the Cu(II) complexes with PrP(106-115) and its Met-to-Ala variants at pH 8.5 (A) and 6.5 (B). All spectra were collected as described in the Experimental Section at 150 K. Experimental data are shown in solid lines, while EPR simulations for the Cu(II)-PrP(106-115) and Cu(II)-PrP(106-115)M109A/M112A complexes, using the parameters listed in Table S1 in the Supporting Information, are shown in dashed lines. Asterisks indicate signals that are associated with free Cu(II) in the buffer solution.

these values are consistent with an equatorial coordination mode of 3N1O according to Peisach-Blumberg correlations.^{104,105} Figure 4B shows the EPR simulation (dotted spectrum) where the superhyperfine splittings from three nitrogen atoms were included, using the parameters listed in Table S1 in the Supporting Information. Finally, it should be noted that adding a sulfur atom as an equatorial or axial ligand did not have a significant effect on the simulated EPR spectrum, since the natural abundance of the ³³S isotope with $I = 3/2$ is very small (0.74%), and therefore, based on continuous wave EPR data, it is

not possible to resolve a superhyperfine interaction with a sulfur atom.

In order to identify the oxygen donor in the Cu(II)-PrP(106-115) complex at pH 6.5, the complex was prepared in ¹⁷O-enriched water. It is well established that the superhyperfine coupling of the ¹⁷O nucleus of a water molecule coordinated to Cu(II) in the equatorial position leads to significant line broadening in the EPR signal of the complex.^{106,107} A

(106) Branden, R.; Denium, J. *FEBS Lett.* **1977**, *73*, 144-146.
 (107) Getz, D.; Silver, B. L. *J. Chem. Phys.* **1974**, *61*, 630-637.

Scheme 1. Protonation Equilibrium for the Cu(II)–PrP(106–115) Complex

comparison of the X-band EPR spectrum of the Cu(II)–PrP(106–115) complex in ^{17}O water at pH 6.5 and that collected in ^{16}O water clearly shows no difference in the line width of the EPR signals (Figure S2 in the Supporting Information). This result suggests that the oxygen atom in the 3N1O coordination mode of this complex is not provided by an equatorial water molecule, but probably by a backbone carbonyl group. It should be noted that the presence of a water molecule coordinated as an axial ligand cannot be discarded, given that the superhyperfine coupling of the ^{17}O nucleus of a water molecule axially coordinated to Cu(II) tends to be very small¹⁰⁷ and cannot be easily identified with this type of experiment.

The EPR data collected on the Cu(II)–PrP(106–115) peptide complex suggest that the equatorial coordination changes from a nitrogen rich environment (a 4N mode) at pH 8.5 to a coordination environment with less nitrogen contribution (a 3N1O mode) at pH 6.5. This implies that the single protonation equilibrium observed by CD is associated with the protonation of a backbone amide of the peptide chain that changes the equatorial coordination from 3N1O at pH 6.5 to 4N at pH 8.5. Plausible models for such coordination modes are shown in Scheme 1. Consistently, EPR data collected on the Cu(II)–PrP(106–115) peptide complex at pH 7.5 reflects the presence of both components and the EPR spectrum at pH 7.5 can be simulated as a mixture of the spectra collected at pH 8.5 and 6.5 (data not shown).

2. Cu(II) Binding to the PrP(106–115) Fragment: Evaluating the Role of the C-Terminal Residues. **2.1. Comparison of Cu(II) Binding to the PrP(106–111) and PrP(106–115) Fragments.** In order to evaluate the role of the C-terminal residues following the His111 in Cu(II) coordination, the shorter PrP(106–111) peptide fragment was titrated by Cu(II) and followed by CD. The CD spectra of the Cu(II) complexes at pH 8.5 and 6.5 (Figures 5A and 5B, respectively) are clearly identical to those obtained upon the Cu(II) coordination to the larger PrP(106–115) peptide (Figures 1B and 1F). This indicates that the pH equilibrium described above is also present in the Cu(II)–PrP(106–111) complex, and it must involve a backbone amide group that precedes the His111. Moreover, EPR data on the Cu(II)–PrP(106–111) complex at pH 6.5 and 8.5 (Figure S3 in the Supporting Information) display EPR parameters that correlate to a change in equatorial coordination mode from 3N1O to 4N upon an increase in pH, similar to that observed for the larger peptide PrP(106–115). Overall, these data indicate that the Cu(II) complex formed with the shorter PrP(106–111) peptide has essentially the same coordination environment as with the larger PrP(106–115) peptide, and therefore, the

residues following His111 (Met-Ala-Gly-Ala) do not participate in Cu binding.

2.2. Effect of the K110P Substitution in the Cu(II) Binding Properties to the PrP(106–115) Fragment. In order to evaluate if the deprotonation of backbone amide groups that precede the His111 is involved in the Cu(II) coordination to the PrP(106–115) fragment, the PrP(106–115)K110P variant was prepared. The PrP(106–115)K110P peptide was titrated by Cu(II) and followed by CD at pH 8.5 and 6.5 (Figures 5C and 5D, respectively). At pH 8.5 a positive signal at $\approx 39000\text{ cm}^{-1}$, less intense signals at $\approx 33000\text{ cm}^{-1}$ and $\approx 29000\text{ cm}^{-1}$, and a negative signal at $\approx 16500\text{ cm}^{-1}$ grow upon addition of Cu(II) (Figure 5C). The titration at pH 6.5 (Figure 5D) displays the same signals as those observed at pH 8.5 (Figure 5C), but with less intensity. At both pH values, the signals do not correspond to free Cu(II) solution (green spectra in Figures 5C and 5D), and they are very different from those observed for the PrP(106–111)–Cu(II) (Figures 5A and 5B) and PrP(106–115)–Cu(II) complexes (Figures 1B and 1F). On the other hand, EPR data on the Cu(II) complex with PrP(106–115)K110P at pH 8.5 displays a g_{\parallel} value of 2.244 and a hyperfine splitting of $A_{\parallel} = 155 \times 10^{-4}\text{ cm}^{-1}$, indicative of an equatorial coordination mode with a lower content of nitrogen ligands (possibly 2N2O), as compared to the Cu(II) complexes with PrP(106–111) and PrP(106–115). These results clearly indicate that the substitution of Lys110 by Pro yields a Cu(II) coordination that is distinctly different from that observed for the PrP(106–115) complex.

Overall, the study of the Cu(II) binding to the shorter PrP(106–111) peptide and the PrP(106–115)K110P variant yields the important conclusion that residues following His111 are not required for Cu(II) binding to His111, and that the pH equilibrium associated with the Cu(II)–PrP(106–115) complex must involve amide groups that precede His111, consistent with the model structures proposed in Scheme 1.

3. Cu(II) Coordination to the PrP(106–115) Fragment: Evaluating the Role of Methionines. In order to evaluate the role of methionines in Cu(II) coordination to PrP(106–115), Met109 and/or Met112 to Ala variants were prepared and titrated by Cu(II), as followed by EPR, UV–vis absorption and CD spectroscopy.

3.1. Effect of the M109A and M112A Substitutions in the Cu(II) Binding Properties to the PrP(106–115) Fragment, as Followed by UV–Vis Absorption and CD. The comparisons of the UV–vis absorption (Figure 6A) and CD spectra (Figure 6B) of the Cu(II) complexes with the PrP(106–115) fragment and the Met-to-Ala variants at pH 8.5 show no significant differences; the spectra display

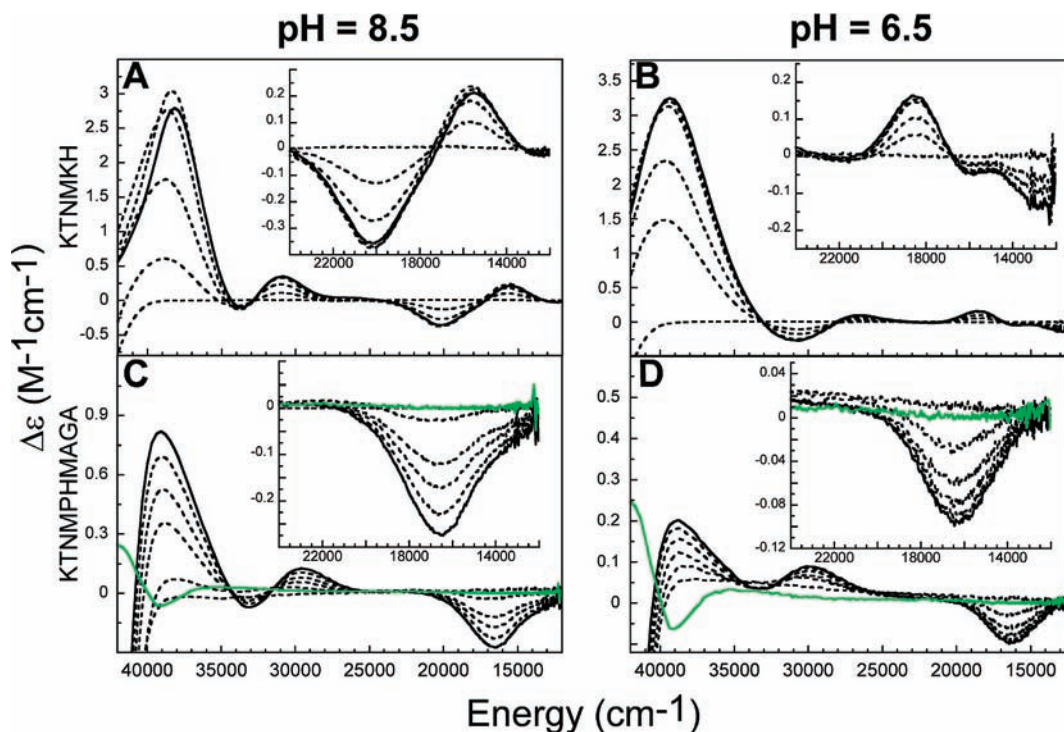


Figure 5. Titration of the PrP(106–111) fragment (KTNMKH) by Cu(II) at pH 8.5 (A) and 6.5 (B), and the PrP(106–115)K110P variant (KTNMPHMAGA) at pH 8.5 (C) and 6.5 (D), as followed by circular dichroism. Only the spectra recorded after the addition of 0, 0.2, 0.4, 0.6, 0.8 equiv (all in dotted lines) and 1.0 equiv (solid lines) of Cu(II) are displayed. A close-up of the lower energy region is shown in the inset for each figure.

essentially the same transitions that are characteristic of the deprotonated form of the complex. The Cu(II) complex with the PrP(106–115)M109A/M112A peptide is the only one that displays some transitions shifted to higher energy, particularly the ligand field envelope and the LMCT band at $\approx 31500\text{ cm}^{-1}$ in the absorption spectrum (black spectrum, Figure 6A), and the positive d–d transition at 15800 cm^{-1} in the CD (black spectrum, Figure 6B, inset). Such an increase in energy for these transitions may indicate a mild increase in the ligand field strength at the metal ion for the Cu(II)–PrP(106–115)M109A/M112A complex. It should be noted that this effect becomes evident only for the peptide where both Met residues have been replaced to Ala, while single Met-to-Ala substitutions have no significant effects.

At pH 6.5, the UV–vis absorption (Figure 6C) and CD spectra (Figure 6D) of the Cu(II) complexes have the same overall shape, and display transitions that are characteristic of the protonated form of the complex. However, some more significant changes become evident in the CD spectra of the PrP(106–115)M109A and the PrP(106–115)M109A/M112A complexes (red and black spectra in Figure 6D, respectively): the negative LMCT band is shifted to lower energy, and the negative d–d transition is shifted to higher energy, which is indicative of an increase in the ligand field strength. Overall, these results suggest that the M109—but not the M112—participates in Cu(II) binding at low pH.

Finally, the Met-to-Ala substitutions have no effect on the protonation equilibrium of the Cu(II)–peptide complexes, as demonstrated by their pH titration followed by CD (Figure S4 in the Supporting Information). Following the CD spectral changes at 15800 cm^{-1} and at 20833 cm^{-1} (Figures S4D and S4E in the Supporting Information,

respectively), a sigmoidal behavior is obtained for all Cu(II) complexes. While the pK_a associated with the protonation of the Cu(II)–PrP(106–115) complex is 7.50 ± 0.09 , the M109A substitution caused an increase of this pK_a to 7.82 ± 0.09 ; the M112A substitution caused a small decrease to $pK_a = 7.25 \pm 0.06$; and the M109A/M112A variant displayed a $pK_a = 7.63 \pm 0.07$, which is essentially the same as that for the Cu(II)–PrP(106–115) complex.

3.2. Effect of the M109A and M112A Substitutions by EPR. The EPR spectra of the Cu(II) complexes formed with PrP(106–115) and its Met to Ala variants at pH 8.5 and 6.5 are shown in Figures 4A and 4B, respectively; and the corresponding g_{\parallel} values and copper hyperfine splittings A_{\parallel} are listed in Table 2. In all cases, the parallel g and A values are similar to those observed for the Cu(II)–PrP(106–115) complex, and an increase in pH yields a significant increase in A_{\parallel} value and a decrease in g_{\parallel} value for all complexes, consistent with a change in equatorial coordination from 3N1O at low pH to 4N at high pH. It should be noted that the most significant differences are observed for the EPR spectrum of the Cu(II) complex with PrP(106–115)M109A/M112A at pH 8.5 (Figure 4A), which shows more pronounced fine structure in the perpendicular region, and the simulation of the EPR spectrum was achieved including larger superhyperfine splittings from the interaction with the nitrogen donors (Table S1 in the Supporting Information). A similar effect, although much less pronounced, is observed for the Cu(II)–PrP(106–115)M109A/M112A complex at pH 6.5 (Figure 4B). This observation indicates that the interaction of the metal ion with the equatorial nitrogen donors becomes slightly stronger in the Cu(II) complexes with no Met residues. This is consistent with

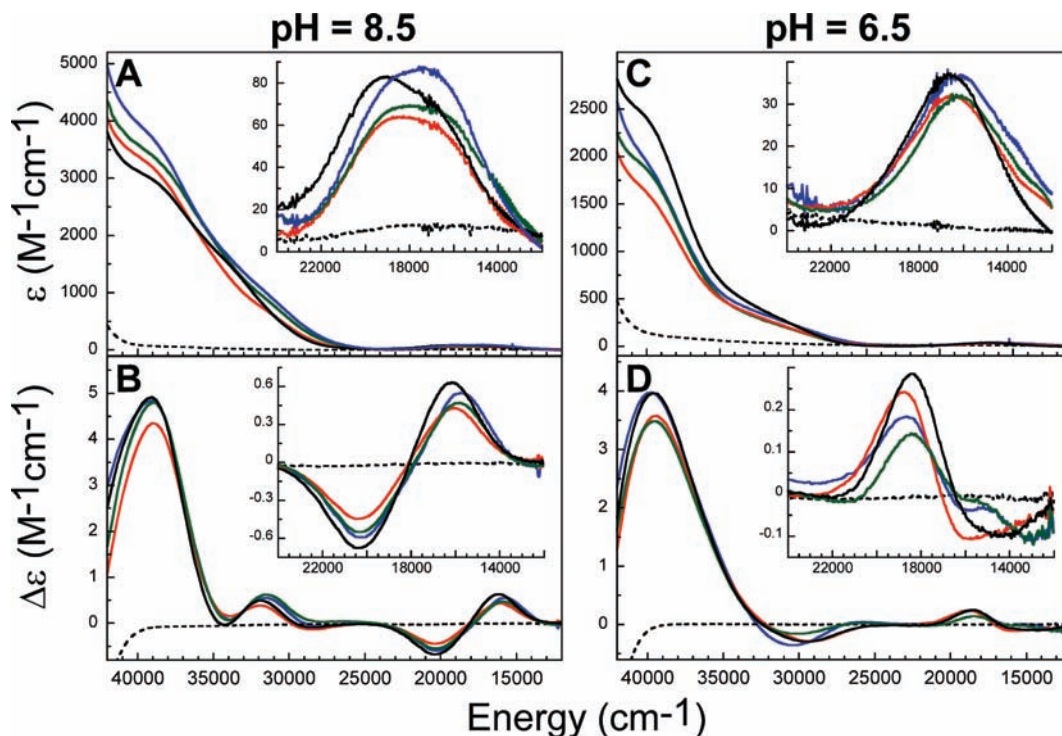


Figure 6. UV-vis absorption spectra of the Cu(II) complexes with PrP(106–115) and its Met-to-Ala variants at pH 8.5 (A) and 6.5 (C). CD spectra of the Cu(II) complexes with PrP(106–115) and its Met-to-Ala variants at pH 8.5 (B) and 6.5 (D). All the spectra were collected after the addition of 1.0 equiv of Cu(II) to each peptide: PrP(106–115) fragment (blue), PrP(106–115)M109A (red), PrP(106–115)M112A (green), and PrP(106–115)M109A/M112A (black) variants.

Table 2. EPR Parameters for the Cu(II) Complexes with the PrP(106-115) Variants at pH 8.5 and 6.5

peptide	pH 8.5		pH 6.5		g_{\parallel}	A_{\parallel} ($\text{cm}^{-1} \times 10^{-4}$) (MHz)
	A_{\parallel}		A_{\parallel}			
	g_{\parallel}	A_{\parallel} ($\text{cm}^{-1} \times 10^{-4}$) (MHz)	g_{\parallel}	A_{\parallel} ($\text{cm}^{-1} \times 10^{-4}$) (MHz)		
PrP(106–115)	2.199	191	573	2.226	167	501
M109A	2.199	190	570	2.228	167	501
M112A	2.197	191	573	2.224	168	504
M109A/M112A	2.193	195	585	2.227	167	501

the increased ligand field observed by CD, and it indicates that the equatorial nitrogen ligands may be compensating for the loss of a weak axial interaction with a Met sulfur atom.

In summary, from the comparison of the Cu(II) complexes with the PrP(106–115) fragment and the Met-to-Ala variants, it derives that (i) regardless of the presence of the Met residues, all Cu(II) complexes display the same protonation equilibrium that involves a conversion from 4N to 3N1O equatorial coordination, with similar values of pK_a (≈ 7.5); (ii) for the protonated form (3N1O) of the complex, the M109A—but not the M112A—substitution leads to an increased ligand field, consistent with the loss of an axial ligand; and (iii) for the deprotonated form (4N) of the complex, only the M109A/M112A variant displays a modest increase in ligand field strength and stronger equatorial nitrogen donors, possibly due to the loss of a weak axial interaction with a Met sulfur atom.

4. Electronic Structure Calculations of Cu(II) Complexes with the PrP(106–113) Peptide. Three different series of coordination models were evaluated by UKS calculations: 4N, 3N and 2N equatorial coordination

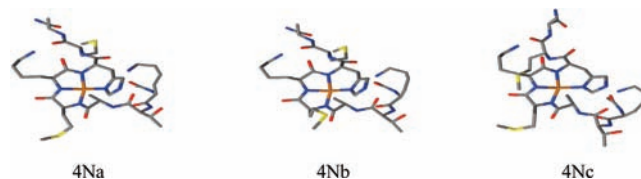


Figure 7. Optimized structures of the three 4N models for the Cu(II)–PrP(106–113) complex. For clarity, H atoms and the side chain of N108 are not shown.

modes, with three, two and one deprotonated amides, respectively, as described below.

4.1. Geometry Optimization of 4N Equatorial Coordination Models. Three different models with a 4N equatorial coordination mode were built, all of them with a Cu(II) ion coordinated to the His111 imidazole nitrogen and the deprotonated amides of His111, Lys110 and Met109. The optimized structures using PBE are given in Figure 7, relevant geometric parameters are listed in Table S2 in the Supporting Information, and the lowest harmonic frequencies of all optimized structures are listed in Table S3 in the Supporting Information. In the optimized structure for the 4Na model, the Cu(II) ion is not coordinated to the Met sulfur atoms, preserving this feature from the initial structure. On the other hand, in the 4Nb and 4Nc models, the Met sulfur atom that was originally coordinated in an axial position moves away from the metal ion: for the 4Nc model the optimized Cu–S distance is 4.5 (LDA) to 4.7 Å (PBE), while for the 4Nb model it ranges from 3.0 (LDA) to 4.8 Å (PBE) (Table S2 in the Supporting Information). The 4Na structure has the lowest energy out of the three optimized structures, although at the GGA level with an implicit

Table 3. Summary of Optimization Results for the 3N and 2N Models of the Cu(II)–PrP(106–113) Complex^d

	initial structure		optimized structure		+ 1 H ₂ O		+ 2 H ₂ O
3N Series							
3Na	3NO No Met	⇒	3NO No Met^b	⇒	3NO No Met^b	⇒	3NO No Met ^{b,d}
3Nb	3NOS _{Met109ax}	⇒	3NS _{Met109eq} O _{ax}	⇒	3NS _{Met109eq} O _{ax}	⇒	3NO No Met^b
3Nc	3NOS _{Met112ax}	⇒	3NO No Met ^c	⇒	3NO No Met ^c	⇒	3NO No Met ^c
3Nd	3NS _{Met109eq}	⇒	3NS _{Met109eq}	⇒	3NS _{Met109eq}	⇒	3NS _{Met109eq}
3Ne	3NS _{Met112eq}	⇒	3NS _{Met112eq}	⇒	3NS _{Met112eq}	⇒	3NS _{Met112eq}
2N Series							
2Na	2N2O No Met	⇒	2N2O No Met ^e	⇒	2NOO_{eqwt}^e	⇒	2NOO_{eqwater}O_{axwt}^e
2Nb	2N2OS _{Met109ax}	⇒	2NOS _{Met109eq} ^f	⇒	2NOS _{Met109eq} O _{axwt} ^g	⇒	2NOS _{Met109eq} O _{axwt} ^g
2Nc	2N2OS _{Met112ax}	⇒	2NOS _{Met112eq}	⇒	2NOS _{Met112eq} O _{axwt} ^g	⇒	2NOS _{Met112eq} O _{axwt} ^g
2Nd	2NOS _{Met109eq}	⇒	2NOS _{Met109eq}	⇒	2NOS _{Met109eq} ^h	⇒	2NOS _{Met109eq} ^h
2Ne	2NOS _{Met112eq}	⇒	2NOS _{Met112eq}	⇒	2NOS _{Met112eq} ^h	⇒	2NOS _{Met112eq} ^h

^a The relative energies of all the structures are given in Tables S5 and S6 in the Supporting Information. The lowest energy optimized structure in each series is in bold. ^b In these structures the distance Cu–S_{Met109} is ≈4.7 Å. ^c In these structures the distances Cu–S_{Met109} and/or Cu–S_{Met112} are ≈4.7 Å, see Table S4 in the Supporting Information for further details. ^d The second water in the 3Na2 structure with two explicit water molecules coordinates axially on the opposite side of the Met109. ^e In these structures the distances Cu–S_{Met} are > 6 Å. ^f At the LDA level these structures did not change their coordination mode and optimized as 2N2OS_{Met ax}. ^g The 2Nb2 and 2Nc2 structures optimize as 2NOS_{Met109eq}O_{axwt} and are lower energy structures, as compared to the 2Nb1 and 2Nc1 structures that optimize as 2NOS_{Met109eq} with no water molecules coordinated to the metal ion. ^h In the 2Nd and 2Ne series, the water molecules do not coordinate to the metal ion, with the exception of the 2Nd2 structure with one water molecule that optimized as 2NOS_{Met109eq}O_{axwt}.

solvation model the energy differences between these structures are small (1 to 3 kcal/mol). These results indicate that when the metal ion adopts a 4N equatorial coordination mode, it can be stabilized with no axial ligand or with a very weak axial interaction with a Met sulfur atom.

4.2. Geometry Optimization of the 3N Equatorial Coordination Models. Five different models with a 3N equatorial coordination mode were built with either Met109 or Met112 participating as either axial or equatorial ligands. All of them have the Cu(II) ion coordinated to the His111 imidazole nitrogen, and the two deprotonated amides of His111 and Lys110. In the 3Na, 3Nb and 3Nc models, the equatorial coordination sphere is completed with an oxygen atom from the backbone carbonyl oxygen of the Asn108 residue. In the 3Na model, the Cu has only the 3NO equatorial ligands, while the 3Nb and 3Nc models are pentacoordinated Cu(II) ions with a 3NOS_{ax} coordination sphere, where the sulfur atom in the axial position comes from Met109 or Met112, respectively. Finally, the 3Nd and 3Ne models are tetraordinated Cu(II) ions with a 3NS equatorial coordination mode, where a sulfur atom from Met109 or Met112 completes the equatorial coordination sphere.

The geometric parameters for all 3N optimized structures are listed in Table S4 in the Supporting Information, and the results are summarized in Table 3. The 3Na, 3Nd and 3Ne models retain the same coordination sphere upon optimization. In contrast, models 3Nb and 3Nc where a Met sulfur atom participates as an axial ligand optimized into very different structures. In the 3Nc model, the sulfur atom from Met112 in the axial position moved away from the copper ion to lead to a 3NO equatorial coordination mode where both sulfur atoms from Met109 and Met112 are placed between 4.2 Å (LDA) and 4.7 Å (PBE) away from the metal ion (Table S4 in the Supporting Information). A very different effect was observed in the 3Nb model, where the sulfur atom from Met109 that was originally in the axial position moved into the equatorial plane, while the backbone

carbonyl oxygen that was originally in the equatorial position moved to the axial position, leading to a 3NS_{Met109eq}O_{ax} coordination sphere. The structure with the lowest energy among this series is the 3Na model with a 3NO equatorial coordination mode, although the Met109 sulfur atom is in the vicinity at ≈4.7 Å from the Cu(II) ion. On the other hand, the 3Nd structure with a 3NS_{Met109eq} coordination mode is very close in energy to the 3Na structure (only 0.33 kcal/mol higher), and thus this model cannot be discarded.

For the 3N series, the coordination of a water molecule in an axial position may be feasible, as observed for the prion octarepeat fragment.³⁰ Therefore, the effect of adding water molecules in the axial positions to the GGA-optimized structures of the 3N series was evaluated. For each structure, a water molecule was added on one side of the plane formed by the 3N equatorial coordination mode and the structures were reoptimized with PBE. When the addition of the first water molecule was performed on the same side as the Met109 residue, the structure labels are followed by number 1 (e.g., 3Nb1), while if the addition is done on the other side of the 3N plane, the structure labels are followed by number 2 (e.g., 3Na2). The geometric parameters for the optimized structures are listed in Table S4 in the Supporting Information, and the results are summarized in Table 3. Overall, adding waters to structures that contain Met sulfur atoms as equatorial ligands (i.e., 3Nb, 3Nd and 3Ne) leads to a significant increase in their relative energy, as compared to the 3NO mode (3Na and 3Nc). This effect is illustrated in Figure 8 for the 3Na, 3Nd and 3Nb coordination modes, while the relative energies for all structures are given in Table S5 in the Supporting Information. Upon addition of one water molecule the 3Nd and 3Nb modes are significantly destabilized relative to the 3Na structure. The energy for the 3Nd structure increases by 7 kcal/mol with respect to the 3Na2 structure upon addition of the first water molecule, while the addition of the second water molecule raises its energy even more (Figure 8, blue trace). Finally, the most striking

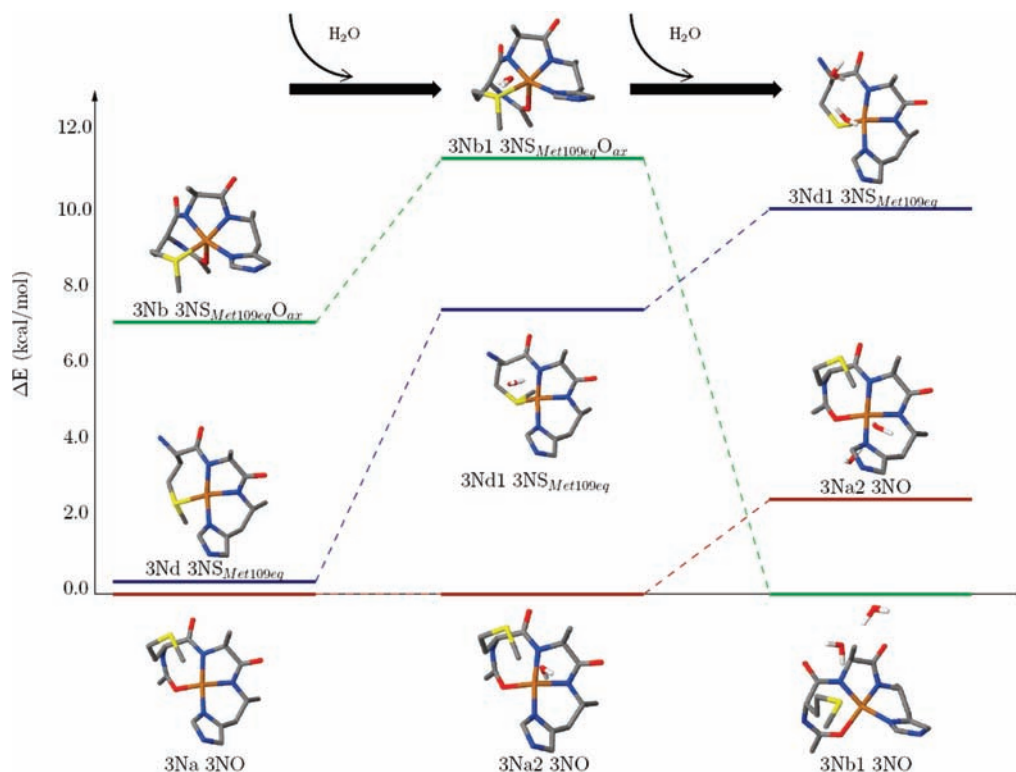


Figure 8. Energy diagram for selected structures of the 3N models of the Cu(II)–PrP(106–113) complex without water (left) and after the successive addition of two explicit water molecules. Most side chains are not shown for clarity; however, the geometry optimizations were done with the complete Cu(II)–PrP(106–113) complex.

ing effect of adding a second water molecule is observed for the 3Nb mode, which converted from a higher energy 3NS_{Met109eq}O_{ax} coordination mode with one water molecule to a 3NO mode with a Cu–S_{Met109} distance of 4.74 Å, and this configuration becomes the lowest energy structure of the series with two water molecules (Figure 8, green trace).

Overall, the theoretical study of the 3N series shows that the addition of explicit water molecules destabilizes the 3N structures that contain Met sulfur atoms in the equatorial position with respect to the 3NO modes. These results suggest that the local effect of the solvent in the Cu(II) coordination does not favor the participation of Met sulfur atoms as equatorial ligands. Moreover, it should be noted that the lowest energy structures of the 3N series with two explicit water molecules (3Nb1, 3Nc1 and 3Na2 structures, Table S5 in the Supporting Information) are within 2.5 kcal/mol and they all have a 3NO equatorial coordination mode and a Met sulfur atom placed ≈ 4.7 Å away from the metal ion. Although the Cu–S distance in these structures is large, these results suggest that the 3NO equatorial coordination mode may be amenable to accommodate a Met sulfur atom as a weak axial ligand.

4.3. Geometry Optimization of the 2N Equatorial Coordination Models. Similarly to the 3N series, five different models with a 2N equatorial coordination mode were built with Met109 or Met112 participating as either axial or equatorial ligands. The initial coordination modes are listed in Table 3. All of them have the Cu(II) ion coordinated to the His111 imidazole nitrogen, and the deprotonated amide of His111. The models 2Na, 2Nb and 2Nc have a 2N2O equatorial coordination mode, the 2Nd and

2Ne models display a 2NOS coordination, while the models 2Nb and 2Nc also have a Met in the axial position.

The optimizations indicate that the 2Na, 2Nd and 2Ne models retain their configuration, while the configuration of the 2Nb and 2Nc models changes dramatically in the PBE optimized structures, leading to a 2NOS_{Met} coordination mode (Table 3). The three lowest energy models 2Nb, 2Nd and 2Na are within 1 kcal/mol (Table S6 in the Supporting Information), indicating that both the 2N2O and 2NSO equatorial coordination modes are feasible. The effect of adding water molecules in the axial positions to the PBE optimized structures of the 2N series was also evaluated, and the results are summarized in Table 3. Similarly to the 3N series, the addition of explicit water molecules to the 2N models has a dramatic effect on their relative energies. Overall, adding waters to structures that contain Met sulfur atoms as equatorial ligands (2Nb and 2Nd) leads to a significant increase in their relative energy (Table S6 in the Supporting Information), as compared to the 2N2O mode (Figure S5 in the Supporting Information). In contrast, the 2Na structure becomes the lowest energy structure in the series, as it is stabilized upon the coordination of an equatorial water and a second water molecule in the axial position. These results clearly indicate that the local effect of the solvent in Cu(II) coordination does not favor the participation of Met sulfur atoms as equatorial ligands, but it favors the coordination of equatorial and axial water molecules for a 2N2O coordination mode.

4.4. Comparison to Experimental EPR Data. The EPR parameters for all 2N, 3N and 4N theoretical models described above were calculated using ORCA with the nonempirical hybrid functional PBE0. The parameters

Table 4. EPR Parameters of Selected Optimized Structures of the 4N, 3N and 2N Models for the Cu(II)–PrP(106–113) Complex^a

ID	g tensor			A tensor		
	g_{xx}	g_{yy}	g_{zz}	A_{xx}	A_{yy}	A_{zz}
4N Set						
4Na	2.048	2.058	2.189	-22.45	18.51	-513.46
4Nc	2.048	2.053	2.182	-14.15	-8.73	-529.33
4Nb	2.041	2.056	2.18	10.15	-38.76	-534.12
3N Set						
3Na	2.049	2.082	2.207	53.86	120.5	-423.58
3Nd	2.042	2.081	2.202	-20.96	55.08	-457.53
3Nb	2.053	2.059	2.189	-7.74	-15.53	-531.59
3Nc	2.048	2.081	2.206	61.34	149.43	-421.10
3N Set + 1 H ₂ O						
3Na2	2.047	2.082	2.208	55.06	129.36	-417.38
3Nd1	2.044	2.103	2.223	13.7	106.81	-393.68
3Nb1	2.053	2.061	2.186	-6.73	-15.98	-529.63
3Nc1	2.051	2.078	2.207	55.91	120.23	-440.51
3N Set + 2 H ₂ O						
3Nb1	2.053	2.076	2.206	44.93	92.86	-450.92
3Na2	2.061	2.073	2.215	33.36	60.16	-490.05
3Nd1	2.031	2.112	2.214	-22.65	146.4	-398.94
3Nc1	2.052	2.078	2.208	52.30	115.78	-450.99
2N Set						
2Nb	2.061	2.065	2.216	6.13	26.7	-464.64
2Nd	2.029	2.097	2.199	38.04	147.09	-299.05
2Na	2.063	2.082	2.236	4.28	-33.52	-544.52
2N Set + 1 H ₂ O						
2Na2	2.061	2.1	2.243	13.28	93.46	-472.7
2Nb2	2.07	2.104	2.253	12.74	100.01	-447.16
2Nd1	2.054	2.091	2.224	55.38	101.14	-370.07
2N Set + 2 H ₂ O						
2Na2	2.014	2.097	2.145	-2.42	236.77	-270.03
2Nb2	2.047	2.053	2.154	53.14	74.49	-338.17
2Nd1	2.026	2.043	2.133	49.82	80.81	-279.55

^a The **g** and **A** tensors were calculated with the nonempirical hybrid functional PBE0. The **A** tensor components are reported in MHz. For each set, the structures are listed in ascending order of their relative energies. Complete listings of relative energies for the 3N and 2N series are in Tables S5 and S6 in the Supporting Information.

for selected 2N, 3N and 4N models are listed in Table 4. At pH 8.5, an experimental g_z value = 2.199 and a hyperfine splitting $A_z = 191 \times 10^{-4} \text{ cm}^{-1} = 573 \text{ MHz}$ is associated with the PrP(106–115)–Cu(II) complex, and a definitive assignment of the equatorial coordination cannot be made from Peisach–Blumberg correlations. However, a detailed comparison of the experimental g_z and A_z values at pH 8.5 with the calculated data listed in Table 4 clearly shows that all 4N structures fall close to the experimental values, indicating that the 4N structures are plausible models for the complex at high pH. The difference between the experimental and theoretical data for the 4N models ranges from 0.010 to 0.019 for g_z , and 38 to 59 MHz (12.6 to $19.6 \times 10^{-4} \text{ cm}^{-1}$)

for A_z ; these differences are within the error of this type of calculations.^{108–110}

In addition, the 3Nb structures with one explicit water molecule and no water molecules also lead to EPR parameters that resemble the experimental data at pH 8.5; however, these two structures are at higher energy (7 and 11 kcal/mol, respectively) relative to the lowest energy structure 3Na (Figure 8), and thus, they may be discarded as probable models. Finally, further support for discarding the 3Nb model with a $3\text{N}_{\text{Met109eq}}\text{O}_{\text{ax}}$ configuration comes from experimental UV–vis absorption and CD data, as no significant changes are observed upon substitution of the Met residues to Ala (Figures 6A and 6B). No other 3N or 2N modes resemble the experimental values in both g_z and A_z . Thus, a 3N coordination mode can be discarded as a plausible model for the deprotonated form of the complex at pH 8.5.

The three 4N structures are very close in energy, all within 3 kcal/mol. While 4Na is the lowest energy structure, the best fit of the experimental data, particularly for the A_z value, is achieved by the 4Nb and 4Nc models, where one Cu–S_{Met} distance is $\approx 4.7 \text{ \AA}$. These results suggest that a very weak axial interaction with one Met sulfur atom may be required to have the best agreement with the experimental EPR parameters. This is consistent with the experimental data at pH 8.5, where the M109A and M112A substitutions alone led to no significant spectral changes, while the double substitution M109A/M112A led to a small shift in the ligand field region of the optical spectra (Figures 6A and 6B) and a better resolution of the nitrogen superhyperfine splittings in the EPR spectrum (Figure 4A). These minor spectral changes could be consistent with a model where one of the Met residues participates as a weak axial ligand in a 4N complex at pH 8.5.

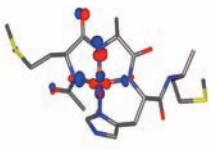


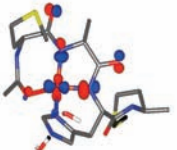
At pH 6.5, an experimental g_z value = 2.226 and a hyperfine splitting $A_z = 167 \times 10^{-4} \text{ cm}^{-1} = 501 \text{ MHz}$ is associated with the PrP(106–115)–Cu(II) complex. These values suggest an equatorial coordination of 3N1O. A detailed comparison of the experimental g_z and A_z at pH 6.5 with the calculated values, listed in Table 4, clearly shows that none of the 4N structures fall close to the experimental values. In contrast, the 3Nb1, 3Na2 and 3Nc1 structures with two water molecules lead to a much better agreement with the experiment, they have a 3NO coordination mode with a Cu–S_{Met} distance of $\approx 4.7 \text{ \AA}$ and they are all within 2.5 kcal/mol (Table S5 in the Supporting Information). The difference between the experimental and calculated data ranges from 0.010 to 0.019, for g_z , and 11 to 50 MHz (i.e., 3.7 to $16.7 \times 10^{-4} \text{ cm}^{-1}$), for A_z . The best fit of both, experimental g_z and A_z values, is given by the 3Na2 model, where the Cu–S_{Met109} distance is 4.81 Å, and one water molecule may be coordinated to the metal ion (Cu–O distance is 3.03 Å, Table S4 in the Supporting Information) in the axial position opposite to the Met109 sulfur atom. These results suggest that a very weak axial interaction with Met109 sulfur atom and the coordination of a water molecule in the axial position are required for the best agreement with the experimental EPR parameters. This is consistent with the experimental CD data, where only the M109A substitution has an effect on the ligand field region of the Cu(II)–PrP(106–115) complex at pH 6.5 (Figure 6D).

(108) Neese, F. *J. Chem. Phys.* **2001**, *115*, 11080–11096.

(109) Neese, F. *J. Chem. Phys.* **2003**, *118*, 3939–3948.

(110) Patchkovskii, S.; Ziegler, T. *J. Am. Chem. Soc.* **2000**, *122*, 3506–3516.

Table 5. Spin Densities and Spin β -LUMO Composition from Loewdin's Population Analysis (LPA) of Selected 4N and 3N Models for the Cu(II)–PrP(106–113) Complex, as Calculated with the PBE and the PBE0 Functionals^a

ID		PBE		PBE0		LUMO β^b
		Spin density	β -LUMO composition	Spin density	β -LUMO composition	
4Na	Cu	45.4	45.7	56.5	56.7	
	N1-Im	3.4	3.0	3.2	2.7	
	N2-H111	7.6	6.5	7.2	5.4	
	N3-K110	18.3	15.4	16.7	12.9	
	N4-M109	9.5	8.1	8.7	6.6	
	O1-M109	5.6	5.6	2.7	3.0	
	O2-N108	1.6	1.8	0.4	0.8	
	S1-M109	0.1	0.2	0.0	0.0	
S2-M112	0.0	0.0	0.0	0.0		
4Nb	Cu	45.7	46.0	56.5	56.9	
	N1-Im	3.8	3.4	3.6	3.0	
	N2-H111	7.6	6.5	7.2	5.5	
	N3-K110	17.6	14.8	16.2	12.4	
	N4-M109	10.5	8.9	9.6	7.3	
	O1-M109	4.8	4.9	1.9	2.3	
	O2-N108	1.6	1.8	0.5	0.8	
	S1-M109	0.0	0.0	0.0	0.0	
S2-M112	0.0	0.0	0.0	0.0		
3Nb1 + 2 H ₂ O	Cu	45.0	45.1	58.0	58.0	
	N1-Im	4.3	3.8	4.4	3.5	
	N2-H111	17.5	14.7	16.5	12.8	
	N3-K110	9.8	8.5	9.0	6.9	
	O1-N108	3.2	3.0	2.5	2.4	
	O2-K110	6.6	6.5	3.1	3.1	
	O3-M109	4.4	4.4	1.7	1.9	
	S1-M109	0.0	0.0	0.0	0.0	
S2-M112	0.0	0.0	0.0	0.0		
3Na2 + 2 H ₂ O	Cu	45.7	45.8	58.6	58.5	
	N1-Im	4.3	3.8	4.3	3.5	
	N2-H111	15.7	13.2	14.8	11.4	
	N3-K110	10.9	9.3	9.6	7.5	
	O1-N108	4.3	3.9	3.4	3.0	
	O2-K110	5.3	5.3	2.0	2.2	
	O3-M109	5.1	5.0	2.6	2.6	
	S1-M109	0.4	0.4	0.0	0.1	
S2-M112	0.0	0.0	0.0	0.0		

^a N1-Im refers to the imidazole nitrogen; N2-H111, N3-K110 and N4-M109 refer to the deprotonated amide nitrogens of the His111, Lys110 and Met109 residues, respectively, that coordinate the metal ion; in the 4N models, O1-M109 and O2-N108 refer to the carbonyl oxygens that form peptide bonds with the amide nitrogens of Lys110 and Met109, respectively; in the 3N models, O1-N108 corresponds to the backbone carbonyl O that coordinates to Cu, while O2-K110 and O3-M109 refer to the carbonyl oxygens that form peptide bonds with the amide nitrogens of His111 and Lys110, respectively; S1-M109 and S2-M112 refer to the thioether S atoms of Met109 and Met112, respectively. ^b The LUMO β pictures were generated from the calculations with the PBE functionals.

Finally, among the 2N series, the 2Na and 2Nb structures lead to parameters similar to the experimental values at pH 6.5, although with a poor fit of the A_z value. The 2Nb structure with a $2\text{NO}_{\text{Met109eq}}$ coordination mode may be discarded due to its destabilization after the addition of water molecules. Further support for discarding equatorial Met coordination comes from experimental EPR, UV–vis absorption and CD data (section 3). On the other hand, the 2Na structure can be discarded because upon addition of water molecules it adopts $2\text{NO}_{\text{eqwater}}$ coordination modes, while ¹⁷O EPR experiments at pH 6.5 indicates water molecules do not participate as equatorial ligands to Cu(II) (Figure S2 in the Supporting Information).

In summary, it can be concluded that a 4N equatorial coordination mode is the best model for the data at pH 8.5, as represented by the 4Nb and 4Nc models; while a 3NO equatorial coordination mode is the best model for the data at pH 6.5, as represented by the 3Nb1, 3Nc1 and 3Na2 models with two explicit water molecules.

4.5. Electronic Structure of the Cu(II)–PrP(106–113) Complexes. The atomic contributions to the spin density

and the β -LUMO composition from Mulliken's (MPA) and Loewdin's (LPA) population analysis for selected 4N and 3N models were calculated with the PBE and PBE0 exchange-correlation functionals; only the LPA values are displayed in Table 5, since MPA yields very similar results. It should be noted that for a given population analysis the spin densities and the β -LUMOs have the same atomic contributions, indicating an almost complete cancellation of the doubly occupied orbitals. The β -LUMOs are used in Table 5 to obtain a better agreement with the spin densities since the α -HOMOs spread more along the complex. Finally, it should be noted that the PBE0 functional predicts less covalent bonds than the faster decaying PBE effective potential; this is because it has some exact exchange in the effective potential that lowers the orbital energies, which in turn localizes the molecular orbitals. Also, the values reported in Table 5 clearly indicate that the unpaired electron is mainly located on the metallic center (atomic contribution for Cu is 56–58% with PBE0) with $3d_{x^2-y^2}$ character, followed by the deprotonated amide nitrogen atoms that together amount to $\sim 33\%$ of the spin density in the 4N

models and ~25% in the 3N models. Smaller contributions are observed for carbonyl oxygen atoms (2.5 to 3.4%) that complete the equatorial coordination in the 3N models, while the contribution from the imidazole nitrogen atoms ranges from 3.2 to 4.4%, consistent with previous electronic structure calculations of Cu sites with imidazole ligands.^{32,111,112} Finally, it should be noted that the contributions from the Met sulfur atoms are almost negligible, consistent with their participation as very weak axial ligands.

The figures corresponding to the β -LUMOs, as depicted in Table 5, show that the most covalent Cu–ligand interactions involve the $3d_{x^2-y^2}$ of Cu and the deprotonated amide nitrogens. The electron pair of the deprotonated amide N atoms are in a hybrid orbital that is mostly sp^2 in nature, with a very small sp^3 contribution. A deprotonated amide can have two resonant structures: one with the lone pair at the negatively charged N atom, and another one where the electron pair (and thus, the negative charge) is located at the carbonyl oxygen atom while the nitrogen forms a double bond with the carbon atom; this resonance would allow for some delocalization of the spin density onto the carbonyl oxygen. This is particularly evident for the amides that form the most covalent bonds with the metal ion; for example, the carbonyl oxygen O1-M109 that forms the peptide bond with the amide nitrogen N3-K110 in the 4N models displays 1.9 to 2.7% of the total spin density, practically just as much as the imidazole nitrogen that is directly coordinated to the Cu ion. Similarly, in the 3N models the carbonyl oxygens O2-K110 and O3-M109 that form peptide bonds with the amide nitrogens N2-H111 and N3-K110, respectively, also display 1.7 to 3.1% of the total spin density.

Finally, it is noteworthy that the Cu–N bond that arises from the interaction with the deprotonated amide is far more covalent (2 to 5 times) than the Cu–N bond formed with the imidazole nitrogen. This is also reflected in the superhyperfine coupling values that were needed for the EPR simulations (Table S1 in the Supporting Information), which are in good agreement with the calculated nitrogen A tensors (Table S7 in the Supporting Information). However, some Cu–N_{amide} bonds are more covalent than others, depending on the coordination mode: in the 4N models, the most covalent Cu–N bond corresponds to the Cu–N_{amide} interaction with the Lys110 amide, followed by the Cu–N_{amide} formed with the Met109, while the Cu–N_{amide} interaction with the His111 amide is the least strong. On the other hand, in the 3N models, the most covalent Cu–N_{amide} bond is formed with the His111 amide, while the Cu–N_{amide} interaction with the Lys110 is less strong. In both cases, the strongest Cu–N_{amide} bond is in a *trans* position to the weakest equatorial bond: the Cu–N_{imidazole} bond for the 4N structures, and the Cu–O bond formed with a carbonyl group in the 3N structures. The highly covalent Cu–N equatorial bonds in these complexes may explain the fact that the interactions with potential axial ligands, such as the Met109 sulfur atom, are very weak.

Discussion

Cu(II) Binding to His111: The Role of Protons. A proton equilibrium associated with the Cu(II)–PrP-(106–115) complex that involves the protonation of a backbone amide of the peptide chain with a pK_a of 7.5 has been identified. Different spectroscopic techniques in combination with electronic structure calculations indicate that the protonated form of the complex has an equatorial coordination 3N1O that changes to 4N upon deprotonation of the backbone amide group (Scheme 1). These findings imply that the coordination environment around Cu(II) bound to His111 at physiological pH is a mixture of these two species. Several studies have aimed at determining the affinity of Cu(II) for His111^{28,51,56,113–115} and/or evaluating the role of methionine residues^{50,60,62,64,65} at pH 7.4 in peptide fragments or in the full length prion protein, leading to very contrasting results. Having a mixture of two species at this pH may have obscured the data analysis of such studies. Thus, our study underscores the importance to consider the different protonation states of the Cu(II) complex that may coexist at a given pH, particularly when drawing conclusions regarding Cu(II) binding affinities or when comparing a binding site in a peptide fragment to the metal binding sites in the whole prion protein.

PrP^C is anchored on the surface of neurons, predominantly on presynaptic membranes.^{116,117} As Cu is released at the synapse, PrP^C is exposed to a range of Cu(II) concentrations.^{117–119} Moreover, cellular studies show that Cu(II) and Zn(II) stimulate endocytosis of PrP,^{10,11} taking the protein from the extracellular space at pH 7.4 to the interior of the endosomes, where pH is low (4 to 5). Thus, PrP^C is exposed to a wide range of Cu(II) and proton concentrations, and consistently, it can accommodate different coordination modes in a pH-dependent fashion. This is the basis for the proposal that PrP^C may function as a Cu sensing protein and it may be involved in Cu uptake into the cell.^{11,12} Our results supports this notion, as the His111 Cu(II) binding site displays 3N1O and 4N coordination modes at physiological pH. The participation of deprotonated backbone amide groups in these coordination modes provides the basis for a pH-dependent Cu coordination behavior. The nitrogen donor of a backbone amide group usually displays high pK_a values (~15). However, it is well documented that binding of Cu(II) leads to backbone amide deprotonation at neutral pH in small peptide complexes, lowering its pK_a value to as low as 4.^{120–122} The assignment of the pK_a of

(113) Davies, P.; Marken, F.; Salter, S.; Brown, D. R. *Biochemistry* **2009**, *48*, 2610–2619.

(114) Nadal, R. C.; Davies, P.; Brown, D. R.; Viles, J. H. *Biochemistry* **2009**, *48*, 8929–8931.

(115) Kozłowski, H.; Luczkowski, M.; Remelli, M. *Dalton Trans.* **2010**, *39*, 6371–6385.

(116) Herms, J.; Tings, T.; Gall, S.; Madlung, A.; Giese, A.; Siebert, H.; Schürmann, P.; Windl, O.; Brose, N.; Kretzschmar, H. *J. Neurosci.* **1999**, *19*, 8866–8875.

(117) Vassallo, N.; Herms, J. *J. Neurochem.* **2003**, *86*, 538–544.

(118) Hopt, A.; Korte, S.; Fink, H.; Panne, U.; Niessner, R.; Jahn, R.; Kretzschmar, H.; Herms, J. *J. Neurosci. Methods* **2003**, *128*, 159–172.

(119) Kardos, J.; Kovacs, I.; Hajos, F.; Kalman, M.; Simonyi, M. *Neurosci. Lett.* **1989**, *103*, 139–144.

(120) Sigel, H.; Martin, R. B. *Chem. Rev.* **1982**, *82*, 385–426.

(121) Sívágó, I.; Osz, K. *Dalton Trans.* **2006**, 3841–3854.

(122) Kozłowski, H.; Kowalik-Jankowska, T.; Jezowska-Bojczuk, M. *Coord. Chem. Rev.* **2005**, *249*, 2323–2334.

(111) Solomon, E. I.; Szilagyi, R. K.; DeBeer George, S.; Basumallick, L. *Chem. Rev.* **2004**, *104*, 419–458.

(112) Quintanar, L.; Yoon, J.; Aznar, C. P.; Palmer, A. E.; Andersson, K. K.; Britt, R. D.; Solomon, E. I. *J. Am. Chem. Soc.* **2005**, *127*, 13832–13845.

7.50 to the amide nitrogen of the Met109 residue is further supported by the fact that the Met109Ala substitution causes an increase in this pK_a value to 7.82, due to the substitution of the more electron drawing thioether group by a methyl group that stabilizes the protonated form of the amide group due to its inductive effect. This effect is also clearly seen in the pK_a values of the amino groups of the free amino acids: the pK_a value of the free amino group for Ala is larger (9.69) than that for Met (9.21). On the other hand, it is interesting to note that, although Met112 does not participate in the Cu(II) coordination sphere, the Met112Ala substitution causes a small decrease of the pK_a of the complex (from 7.50 to 7.25). This small effect can be explained considering that the protonated form of the complex has a 3N1O coordination mode with two deprotonated amides, and thus, it has no total charge; while the deprotonated form holds a 4N coordination mode with three deprotonated amides, and it has a total charge of -1 . Consequently, having the negative dipole of the thiol group of a Met residue in the vicinity would disfavor the negative form of the complex (4N), and thus, its replacement with a methyl group would shift the equilibrium toward the 4N coordination mode, lowering the pK_a value. Therefore, while the Met109Ala substitution has a direct effect in the pK_a of its backbone amide group, the Met112Ala substitution has only an indirect effect on the 3N1O–4N equilibrium.

Cu(II) Binding to His111: The Role of Methionine Residues. The His111 binding site is unique in the sense that it is the only Cu binding site in the human prion protein that has methionine residues in the vicinity. In particular, the role of Met109 and Met112 as Cu(II) ligands has been previously proposed, suggesting equatorial coordination of one or both of these Met residues,^{50,64,65} however, the effect of pH on Cu(II) coordination to His111 was not studied in these reports, and the spectroscopic measurements were performed at pH values where a mixture of the protonated and deprotonated forms of the Cu(II) complex are present. Our pH-dependent spectroscopic study of Met-to-Ala variants of PrP(106–115), in combination with electronic structure calculations, has established that Met109 and Met112 do not participate as equatorial ligands for Cu(II) bound to His111, and that Met112 is not an essential ligand for Cu. In contrast, Met109 may play a role as a weak axial ligand, particularly at low pH when the equatorial coordination mode is 3NO. For the deprotonated form of the Cu(II) complex, with a 4N equatorial mode, coordination of Met109 as an axial ligand leads to the formation of a six-membered ring, which could in turn contribute to a more stable Cu(II) complex at high pH. Moreover, given that Cu(II) coordination to His111 involves deprotonation of the preceding backbone amide groups, the nature of the residue at position 109 can determine the pK_a associated with the 3NO–4N equilibrium (Scheme 1) that is present at physiological pH, as discussed above. Interestingly, Met109 is highly conserved among mammalian PrP proteins, with the exception of mouse and marsupial PrP;⁶⁷ while Met112 is not conserved, and it is often substituted by Val. Thus, it turns out that evolutionary pressure has maintained at position 109 a Met residue that is capable of completing the Cu(II) coordination sphere as an axial ligand, and it is important to regulate the balance of the two protonation

states of the Cu(II) complex with His111 that are present at physiological pH.

Several reports have suggested that Cu bound to His111 is redox-active. Spin-trapping experiments suggest that the PrP(106–126) fragment is capable of producing hydrogen peroxide in the presence of Cu(II).⁷² A reduction potential of ~ -100 mV (vs NHE) for a quasi-reversible Cu(II)/Cu(I) couple has been reported for the Cu complexes with PrP(106–114) and PrP(91–126) fragments at pH 7.4, and this number is lowered upon removal of Met109 or Met112.^{50,64} It has also been shown that these Cu complexes can produce superoxide in the presence of ascorbic acid and oxygen.⁵⁰ While the nature of the equatorial ligands in the coordination modes that coexist at physiological pH (Scheme 1) is not likely to support reduction to Cu(I), the participation of Met residues as weak axial ligands would certainly contribute to stabilize the reduced form of the complex, as Cu(I) is known to prefer softer ligating atoms like sulfur. In fact, EXAFS studies have demonstrated Cu–S interactions in the Cu(I) complexes of PrP(106–114) and PrP(91–126) fragments at pH 7.4, and a 2(N/O)2S coordination mode has been proposed;⁵⁰ unfortunately at this pH the EXAFS spectra would have contributions from the two different protonation states of the complex, complicating the data analysis and obscuring the coordination mode assignments. The present study demonstrates that Cu(II) complexes with 3NO and 4N equatorial coordination modes with weak axial Met ligands coexist at pH 7.4. Reduction of these Cu(II) species to Cu(I) would certainly strengthen the interaction with the Met sulfur atoms, and it would shift the proton equilibrium of the Cu–peptide complex to favor the 3NO coordination mode over the 4N mode. The decreased positive charge at the metal center could potentially lower the pK_a values associated with the backbone amide's deprotonation to such an extent that the number of deprotonated amide nitrogens may decrease, although this possibility must be assessed by pH-dependent XAS studies. In any case, the strengthened interaction with Met sulfur atoms upon reduction of the Cu complex would lead to a significant decrease in the Cu–S bond length, and hence, a large reorganization energy. Our electronic structure studies suggest that the interaction with the axial Met109 sulfur is so weak that the Cu–S distance is ~ 4.7 Å, while EXAFS studies of the Cu(I)–PrP(106–114) complex indicate a Cu–S distance of ~ 2.3 Å.⁵⁰ Such a large change in Cu–S distance would imply that the site has a very large reorganization energy associated with its reduction. According to the semiclassical theory for intermolecular electron transfer (ET), the rate of ET from a substrate to the active site of a protein is dependent upon several factors, two of them being the driving force and the reorganization energy of the site. Considering that the Cu(II) binding site at His111 would have a very large reorganization energy associated with its reduction to Cu(I), and that the reduction potential associated with this site is negative, the rate of ET would be very slow even in the event that the complex could find an appropriately strong reducing agent. These remarks

(123) Breydo, L.; Bocharova, O. V.; Makarava, N.; Salnikov, V. V.; Anderson, M.; Baskakov, I. V. *Biochemistry* **2005**, *44*, 15534–15543.

lead to the conclusion that the function of this site could not possibly be that of an electron transfer site.

On the other hand, several studies have demonstrated that Met and His residues of PrP^C are susceptible to oxidation.^{14,123–127} Incubation of PrP^C with Cu(II), ascorbic acid and oxygen leads to Met and His oxidation.^{14,126} These observations have led to the proposal that PrP^C possesses antioxidant activity that is related to its ability to sequester Cu(II) ions and support Cu(II) reduction to Cu(I) and activation of oxygen to oxidize surrounding Met and His residues. This way, metal-catalyzed oxidation of PrP^C would be preventing oxidative damage that otherwise free Cu(II) ions would promote in the synaptic cleft. However, the oxidation state of Met residues has an important impact on the fibrillogenic properties of the PrP peptide 106–126 and the full-length recombinant PrP.^{123,124} Accordingly, Cu-catalyzed oxidation of Met residues should have an impact on the fibrillogenic properties of PrP^C; however, the effect of Cu(II) in the conversion of PrP^C to PrP^{Sc} and the nature of the species that is stabilized by Cu(II) are not fully understood.^{128–135} Still, there seems to be consensus in that Cu(II) inhibits *in vitro* conversion of full-length mammalian PrPs into amyloid fibrils,^{128–132} and this effect has been ascribed to Cu(II) binding to the His96/His111 region.¹²⁸

The region encompassing residues 90–140 of the protein is important for the conversion of PrP^C to PrP^{Sc}; it includes the His111 Cu binding site, and several Met residues that are susceptible sites for oxidation. Our study demonstrates that Met109 may play an important role as an axial ligand for Cu(II) bound to His111 that would help stabilize the reduced form of the complex, conferring this site with redox activity. The redox activity of this site may support Cu-catalyzed oxidation of Met residues in the vicinity, which in turn is known to have an important impact in the conversion of PrP^C to PrP^{Sc}. Moreover, it is

interesting to note that the region encompassing residues 109 to 112 (in the human sequence) has been identified as key for the efficiency of prion propagation.¹³⁶ Although Met112 is not conserved among mammalian PrPs, a correlation between infectivity and the presence of a Met residue in position 112 has been reported for Syrian HaPrP and Chinese HaPrP.⁶⁷ On the other hand, Met109 is highly conserved, MoPrP being one of the very few mammalian PrPs that do not have a Met residue at this position.⁶⁷ The substitution of this Met for a Leu in MoPrP has a significant effect on the required incubation time for prion propagation in mice.^{137,138} Thus, it is tempting to propose that Met109 (and possibly Met112 too) may play a crucial role in the conversion of PrP^C to PrP^{Sc}, and possibly in the infectivity of the misfolded isoform. The presence or absence of a Met residue at position 109 (or in other positions such as Met112) in different mammalian PrPs could dictate the nature of the Cu coordination modes, that in turn would determine the extent of the Cu-catalyzed oxidation of the protein, having an effect on the stabilization of a different ensemble of PrP conformations and aggregated isoforms in each species. Further studies on the role that Met109 and Met112 play in the redox activity of the Cu binding site at His111 and the Cu-catalyzed oxidation of Met residues in the vicinity should contribute to our understanding of how this Cu binding site affects the oxidation of PrP^C and its aggregation and amyloidogenic properties.

Acknowledgment. This research was funded by CONACYT (Grant No. J4878Q-1), ICyTDF (Grant No. PIFUTP08-161), and a “For Women in Science Fellowship” awarded by L’Oreal, UNESCO and the Mexican Academy of Sciences (to L.Q.). L.R.-A. has been recipient of postdoctoral fellowships from CONACYT (Grant No. 060366-Q and the program “Estancias Posdoctorales Vinculadas al Fortalecimiento de la Calidad del Posgrado Nacional”); R.G.-A. is recipient of a PhD fellowship from CONACYT; E.B. and S.T. received undergraduate fellowships from CONACYT; and I.L. was supported by CONACYT Grant No. APLIC103687. The authors would like to thank Prof. Martha Sosa and Dr. Alejandro Solano for allowing access to a Bruker ELEXYS 500 EPR system, which was purchased with funds from CONACYT (Grant No. 41128Q); I.Q. Geiser Cuellar for assistance with the acquisition of ES-MS data; and LSVP-UAMI and DGSCA-UNAM for computing time in the servers Aitzalao and KanBalam, respectively.

Supporting Information Available: Simulated CD spectrum for the Cu(II)–PrP(106–115) complex at pH 7.5; ¹⁷O EPR data on the Cu(II)–PrP(106–115) complex at pH 6.5; EPR spectra for the Cu(II) complex with the shorter PrP(106–111) fragment; pH titration of the Cu complexes with the Met-to-Ala variants of PrP(106–115) followed by CD; energy diagram for selected structures of the 2N models; geometric parameters and frequencies for the 4N and 3N optimized structures; relative energies for the 3N and 2N series; and calculated nitrogen A tensors for selected 3N and 4N models. This material is available free of charge via the Internet at <http://pubs.acs.org>. Cartesian coordinates for all optimized structures are available upon request.

(124) Heegaard, P. M. H.; Pedersen, H. G.; Flink, J.; Boas, U. *FEBS Lett.* **2004**, *577*, 127–133.

(125) Requena, J. R.; Dimitrova, M. N.; Legname, G.; Teixeira, S.; Prusiner, S. B.; Levine, R. L. *Arch. Biochem. Biophys.* **2004**, *432*, 188–195.

(126) Requena, J. R.; Groth, D.; Legname, G.; Stadtman, E. R.; Prusiner, S. B.; Levine, R. L. *Proc. Natl. Acad. Sci. U.S.A.* **2001**, *98*, 7170–7175.

(127) Wong, B.-S.; Wang, H.; Brown, D. R.; Jones, I. M. *Biochem. Biophys. Res. Commun.* **1999**, *259*, 352–355.

(128) Bocharova, O. V.; Breydo, L.; Salnikov, V. V.; Baskakov, I. V. *Biochemistry* **2005**, *44*, 6776–6787.

(129) Quaglio, E.; Chiesa, B.; Harris, D. *J. Biol. Chem.* **2001**, *276*, 11432–11438.

(130) Ricchelli, F.; Buggio, R.; Denise Drago, D.; Salmona, M.; Forloni, G.; Negro, A.; Tognon, G.; Zatta, P. *Biochemistry* **2006**, *45*, 6724–6732.

(131) Liu, M.; Li, Y.; Zhou, X.; Zhao, D. *J. Biochem.* **2008**, *143*, 333–337.

(132) Orem, N. R.; Geoghegan, J. C.; Deleault, N. R.; Kascak, R.; Supattapone, S. *J. Neurochem.* **2006**, *96*, 1409–1415.

(133) Tsirolnikov, K.; Rezaei, H.; Dalgalarondo, M.; Chobert, J.-M.; Grosclaude, J.; Haertlé, T. *Biochim. Biophys. Acta* **2006**, *1764*, 1218–1226.

(134) Wong, E.; Thackray, A. M.; Bujdosó, R. *Biochem. J.* **2004**, *380*, 273–282.

(135) Qin, K.; Yang, D.-S.; Yang, Y.; Chishti, M. A.; Meng, L.-J.; Kretzschmar, H. A.; Yip, C. M.; Fraser, P. E.; Westaway, D. *J. Biol. Chem.* **2000**, *275*, 19121–19131.

(136) Moore, R.-A.; Vorberg, I.; Priola, S.-A. *Arch. Virol. Suppl.* **2005**, *187*–201.

(137) Supattapone, S.; Muramoto, T.; Legname, G.; Mehlhorn, I.; Cohen, F. E.; Dearmond, S. J.; Prusiner, S. B.; Scott, M. R. *J. Virol.* **2001**, *75*, 1408–1413.

(138) Vorberg, I.; Groschup, M. H.; Pfaff, E.; Priola, S.-A. *J. Virol.* **2003**, *77*, 2003–2009.